P-06-60

Forsmark site investigation

Determination of porosity and micro fracturing using the ^{14}C-PMMA technique in samples taken from Forsmark area

Laura Penttinen, Marja Siitari-Kauppi, Jussi Ikonen
Laboratory of Radiochemistry, Department of Chemistry,
University of Helsinki

September 2006

Svensk Kärnbränslehantering AB
Swedish Nuclear Fuel
and Waste Management Co
Box 5864
SE-102 40 Stockholm Sweden
Tel 08-459 84 00
+46 8 459 84 00
Fax 08-661 57 19
+46 8 661 57 19

ISSN 1651-4416
SKB P-06-60

Forsmark site investigation

Determination of porosity and micro fracturing using the ^{14}C-PMMA technique in samples taken from Forsmark area

Laura Penttinen, Marja Siitari-Kauppi, Jussi Ikonen
Laboratory of Radiochemistry, Department of Chemistry,
University of Helsinki

September 2006

Keywords: Rock porosity, Micro fracturing, ^{14}C-PMMA method, Image analyses, AP PF 400-03-58.

This report concerns a study which was conducted for SKB. The conclusions and viewpoints presented in the report are those of the authors and do not necessarily coincide with those of the client.

A pdf version of this document can be downloaded from www.skb.se

Abstract

Porosity and micro fracturing were studied in the laboratory using samples taken from the Forsmark site investigation area. The purpose of the study was to determine the porosity pattern of 13 selected rock cores from seven core drilled boreholes. The heterogeneities in porosity according to textural changes in rock minerals were determined.

The samples were studied by using the ^{14}C-PMMA method which gives the spatial distribution of porosity and micro fracturing in the samples. Comparable porosity determinations were made using conventional water gravimetric measurements.

The matrices of rock samples varied from very tight and unaltered having porosities about 0.1% to highly altered and weathered rock which showed high PMMA porosities up to 10%. The average porosities of low porous rock were in the range from 0.1% to 0.5%. The highest porosities were found in the matrices adjacent to water bearing fracture zones which were altered and/or weathered. However, in some cases these zones were non-porous indicating very low permeability.

Sammanfattning

Porositet och mikrosprickbildning har undersökts i prover tagna i Forsmarks platsundersöknings-område. Syftet med undersökningen var att bestämma porositetsfördelningen i 13 utvalda bitar av borrkärna från sju kärnborrhål. Bestämningarna omfattade heterogeniteter i porositeten beroende på förändringar i mineralers textur.

Proverna undersöktes med ^{14}C-PMMA-metoden, vilken ger den rumsliga fördelningen av porositeten och mikrosprickbildningen i proverna. Jämförande porositetsmätningar gjordes med den konventionella vattenmättnadsmetoden.

Provbitarnas karaktär varierade från mycket tätt matrisberg med porositeter runt 0,1 % till kraftigt omvandlade och vittrade bitar med PMMA-porositeter upp till 10 %. Medelporositeten för den oomvandlade bergmatrisen var i storleksordningen mellan 0,1 % till 0,5 %. De högsta porositeterna uppmättes närmast intill vattenförande sprickzoner med omvandlat och/eller vittrat berg. I vissa fall hade dock även det omvandlade berget låg porositet, vilket indikerar låg permeabilitet.

Contents

1 Introduction

This report describes the study of the micro fracturing and porosity of rock core samples from the boreholes KFM01A-KFM05A, KFM06B, and KFM07A by using the ^{14}C-PMMA method (^{14}C-polymethylmethacrylate). The activity is related to the Site Investigation studies in Forsmark. The work is outlined in AP PF-400-03-58 and the method description in detail is given by SKB MD 540.003 (Porositetsbestämning med PMMA). The PMMA method has been in continuous use in 1995–2006 for several applications needed for crystalline rock structure studies.

For the examination 13 cylindrical core samples were delivered to the Laboratory of Radiochemistry (HYRL) having a diameter of c. 5.1 cm and different lengths from 5 cm to 20 cm. The rock types of the samples were granites, granodiorites, tonalities with variations in alteration and weathering products. In addition a few samples were taken adjacent to water bearing fracture zones.

In Table 1-1 controlling documents for performing this activity are listed. Both activity plan and method descriptions are SKB's internal controlling documents.

The results are stored in SKB's data base SICADA, where they are traceable by the Activity Plan number.

Table 1-1. Controlling documents for performance of the activity.

Activity plan	**Number**	**Version**
Provtagning och analyser av borrkärna från KFM01A och KFM02A för bestämning av transportegenskaper	AP PF-400-03-58	1.0
Method descriptions	**Number**	**Version**
Porositetsbestämning med PMMA	SKB MD 540.003	1.0

2 Objective and scope

The main focus of the work was to analyze the porosities and visualize the heterogeneous pore structure of rocks from the Forsmark site investigation area by using the ^{14}C-PMMA method. The method has been used previously to study the porosities and pores structures of different low porous media as well as to study the excavation damaged zones both in the Research Tunnel at Olkiluoto in Finland, the Äspö Hard Rock Laboratory in Sweden and Grimsel Underground Rock Laboratory in Switzerland. The experience from the previous analyses has shown that the technique can be applied effectively to study the spatial distribution of porosity in low porous media. The porosity profiles adjacent to water bearing fracture zones can also be studied.

The objective of the activity is to provide visualisation and quantitative results on,

- interconnected porosities of rock samples,
- porosity profiles of altered zones next to water conducting, or presumptive water conducting fractures,
- micro fracturing of rock samples.

3 Methods

3.1 Sample preparation

The thirteen samples were received at the Laboratory of Radiochemistry, University of Helsinki, HYRL, in two batches. An internal HYRL code was given each core sample (F1–F13) and they were photographed. Appendices 1–13 present the photo images of each sample before any operation. The lengths and widths of the samples and their codes are presented in Table 3-1. Samples F1–F6 and F13 were cut into two or three pieces with a diamond saw to have separate pieces for PMMA analysis and for water gravimetry measurements (see partition diagrams in Appendices 1–6 and 13). The other samples were impregnated without cutting. The sawing scheme for autoradiography after PMMA impregnation is shown in Appendices 1–13. The diamond saw used in the experiment was of the Eurocoup-Masondry type. The thickness of the blade was 1.8 mm and Ø350 mm. The speed of rotation was 2,800 rpm and the loss of rock matrix 2.1 mm. Appendix 14 presents the initial data provided by SKB (Eva Gustavsson, Geosigma) containing a short description of sample types and sampling depths.

3.2 Water gravimetry

Water gravimetry was performed on rock samples F1–F5, F6 and F13 to roughly evaluate the impregnation time needed for thorough intrusion of impregnant. The rock samples F8–F12 were analysed in their entirety, i.e. cutting for water gravimetry subsamples was not considered desirable. The water porosity determined relative to time gives the rate of intrusion, roughly indicating how easily the interconnected pore network is filled with water and also with PMMA. The modified water gravimetry method used here was produced during the development of the PMMA technique and is not a standard method.

Table 3-1. Sample codes, section details, diameters, porosity results from SKB, lengths before sawing, lengths for sawn samples used in PMMA and water gravimetry (H_2O) analysis.

Code HYRL	Code SKB	Secup (m)	Seclow (m)	Diameter (mm)	SKB porosity (%)	Length before sawing (cm)*	PMMA samples (cm)**	H_2O samples (cm)*
F1	KFM01A	486.90	487.10	51	0.19	20	4.1	2.0
F2	KFM02A	275.77	275.90	51	16	13	4.2 and 2.2	2.2
F3	KFM02A	552.23	552.33	51	0.28	10	4.0	1.9
F4	KFM04A	239.75	239.94	51	9.95	19	4.3 and 2.1	2.1
F5	KFM05A	374.60	374.70	51	–	10	8.0	2.0
F6	KFM03A	242.83	242.93	51	–	10.5/11.5	4.0	1.8
F7	KFM04A	204.30	204.35	51	–	4.5/5	4.5/5	–
F8A	KFM04A	359.56	359.85	51	–	5/6.5	5 /6.5	–
F8B						9.5 /11	–	–
F9	KFM05A	206.30	206.43	52	–	10/14.5	10/14.5	–
F10	KFM05A	690.95	691.10	51	–	15	15	–
F11	KFM06B	56.25	56.33	52	–	5	5	–
F12	KFM07A	182.10	182.21	51	–	6.5/11	6.5/11	–
F13	KFM07A	608.82	608.92	51	–	10	4.1	2.0

* lengths as an average

** lengths are taken from the shortest and longest locations

The samples for water gravimetry analysis were desiccated in 105ºC degrees for 7 days. After cooling, they were emerged into milliQ water in separate tubs and weighed every hour during the first day to monitor the impregnation of water inside the rock. The experiment was carried out for 38–42 days. The results for the H_2O samples can be found in Figures 3-1 and 3-2. The uncertainty is about 10%. After approximately two weeks of impregnation the maximum porosity value was reached in low porosity samples. In high porosity samples the intrusion of water was rapid; after one week the constant porosity value was reached, indicating easily attainable interconnected pore networks in these samples.

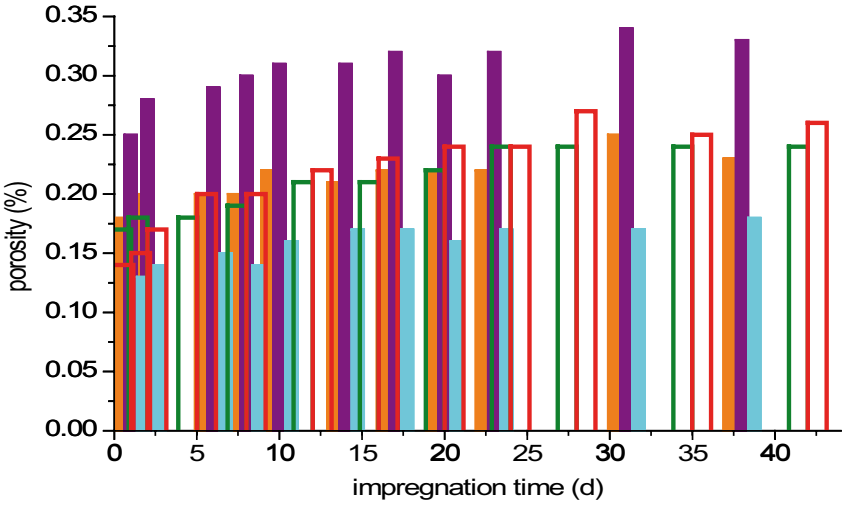

Figure 3-1. *Water gravimetry results for samples F1 (turquoise bar), F3 (green open bar), F5 (red open bar), F6 (orange) and F13 (violet).*

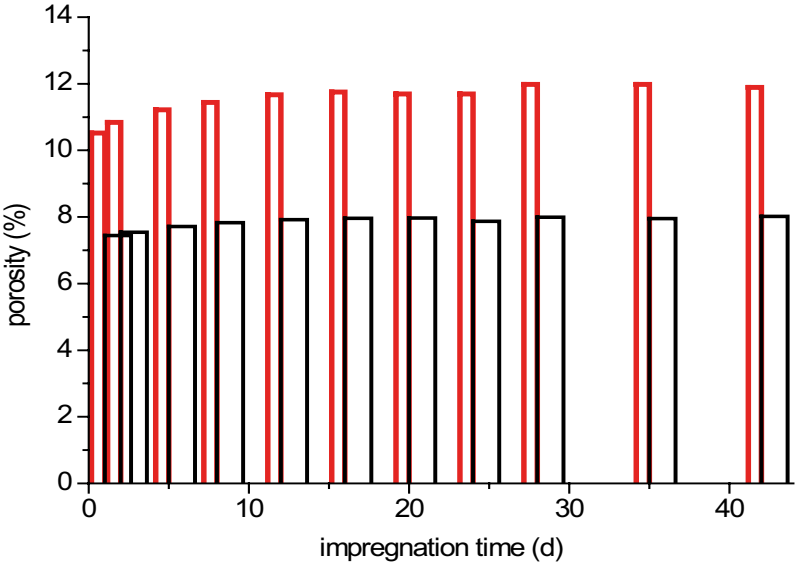

Figure 3-2. *Water gravimetry results for samples F2 (red open bar) and F4 (black open bar).*

3.3 ^{14}C-PMMA method

The ^{14}C-PMMA method involves the impregnation of centimetre-scale rock cores with ^{14}C labelled methylmethacrylate (^{14}C-MMA) in a vacuum, irradiation polymerisation, autoradiography and optical densitometry using digital image-processing techniques /1,2,3,4,5,6/. ^{14}C-MMA, a labelled low-molecular-weight and low-viscosity monomer which wets the silicate surfaces well and which can be fixed by polymerisation, provides information about the accessible pore space in crystalline rock that cannot be obtained using other methods. The method has been described in the report "Use of the ^{14}C-PMMA and He-gas methods to characterize excavation disturbance in crystalline rock" by /7/.

Total PMMA porosity, i.e connected porosity, is calculated by using 2D autoradiographs of the sawn rock surfaces. The geometry of porous regions is then visualised. The conditions for applying this method are: (i) a known local bulk density; (ii) the presence of only two phases, i.e. mineral and PMMA; and (iii) a homogeneous distribution of pores and minerals below the lateral resolution limit of autoradiography.

3.3.1 Properties of ^{14}C-MMA tracer

Methylmethacrylate (MMA) is a monomer with a viscosity 0.00584 Pas (20°C) /8/ that is significantly lower than the viscosity of water 0.00895 Pas (25°C) /9/. Table 3-2 lists the viscosities of the epoxy and acrylic resins used in Swiss experiments /10/ as well as the viscosity of MMA used in this experiment and water. All the resins are widely used for matrix characterization purposes. Because its contact angle on silicate surfaces is low, impregnation of bulk rock specimens by MMA is rapid by capillary forces and dependent on the existing pore apertures. The MMA molecule is small (molecular weight 100.1), it has non-electrolytic properties and only low polarity, the polarity of the ester being considerably lower than that of water. In the rock matrix MMA behaves like a non-sorbing tracer. The low β energy of the carbon-14 isotope, a maximum of 155 keV, is convenient for autoradiography measurements.

The monomer from which the dilutions with inactive MMA (MMA for analyses, Merck) for studies were done was ^{14}C-labelled MMA with a specific activity of 2–5 mCi/g and a radiochemical purity of > 95%. In this study, the dilution of the tracer varied between 37 kBq/ml (1 µCi/ml) and 1,110 kBq/ml (30 µCi/ml). The calibration sources activities ranged from 462 Bq/ml (12.5 nCi/ml) to 185,000 Bq/ml (5 µCi/ml).

Table 3-2. Viscosities of MMA used in this experiment, water, epoxy resin /10/ and acrylic resin used in Swiss experiments /10/.

Resin	viscosity Pa s
MMA	0.00584 (20ºC)
Water	0.00895 (25ºC)
acrylic resin	≈0.03 (5°C), < 0.01(20°C)
epoxy resin	0.15 (13°C), 0.1 (23°C)

3.3.2 Drying, impregnation and irradiation of samples

Samples were vacuum-dried in aluminium chambers for 3–26 days at a maximum temperature of 105°C and then cooled to 18°C. Impregnation with ^{14}C-MMA was carried out by placing the tracer in a 50 ml reservoir and transferring it under vacuum into the impregnation chamber. Slow transfer of the monomer ensures degassing and infiltration of the sample without vapour. Impregnation time varied between 13 and 30 days. After impregnation, samples were irradiated with gamma rays from a Co-60 source to polymerise the monomer in the rock matrix; the dose required was 70 kGy (7 Mrad). Samples were irradiated in glass or polyethylene vials under water and ^{14}C-MMA emulsion. In addition a few highly or moderately porous samples had to be irradiated under active tracer to avoid any outdiffusion of ^{14}C-MMA from the rock sample during irradiation which took from 5 to 7 days. Appendix 15 lists the experimental procedure for the studied samples.

3.3.3 Autoradiography

Irradiation of rocks with Co-60 causes strong thermoluminescence in K-feldspar and other major rock-forming minerals which exposes autoradiography film. To avoid this effect, the thermoluminescence was released by heating the impregnated and irradiated samples to 120°C for a period of 3 hours prior to sawing. Mylar foil with an aluminium coating was used to shield the film from the rest of emissions.

After heating, the samples were sawn into pieces as shown in the partition diagrams (Appendices 1–13). The sawn rock surfaces were exposed on Kodak BioMax MR film, a high-performance autoradiography film for ^{14}C and other low-energy β-emitting nuclides. The nominal resolution of the β film is a few μm. The final spatial resolution achieved depends on the roughness of the sawn surface, the space between the rock and autoradiography film and the range of the 155 keV beta particles in the rock matrix.

With the level of tracer activity and the type of autoradiography film employed, the exposure times for samples ranged from 4 to 25 days. While the short exposure times are convenient for the quantitative determination of porosity, the longer exposure times are better for the qualitative determination of microfracturing. The employed exposure times are listed in Appendix 15.

Sensitivity

The detection system of autoradiography refers to nuclear emulsion of the autoradiography film and the measurement of the blackening of the film by digitizing the intensities (grey levels) of the film. Since the response of the image source and the amplifier of the digital image analysator are linear, the digitised grey levels of the film can be treated as intensities and converted to optical densities, which are defined as decadic logarithm of the intensity ratio of background to sample sub-domains. Thus the blackening is related to silver grain density according to Lambert & Beer's law and is concentration proportional. The linearity of the film autoradiography is much lower than the modern FLA scanner technique, which is described in Chapter 3.4.

The sensitivity of the autoradiography film is declared as a function of exposure time, the activity of the radiation source per square area and the blackening of the autoradiography film. Figure 3-3 shows the effect of exposure time on the optical densities of the ^{14}C-PMMA calibration sources, which are dilutions of the used tracer. An example of an autoradiograph of 5 days exposed calibration sources is included. The nonlinear response of the autoradiography method at high concentrations can be seen and the saturation of the autoradiography film at optical density values of around 1.8 is detected. For one day exposure, linearity is kept through the activity range. For longer exposure times, curves are composed of two slopes that underscore the nonlinear response of the nuclear emulsion at high concentrations.

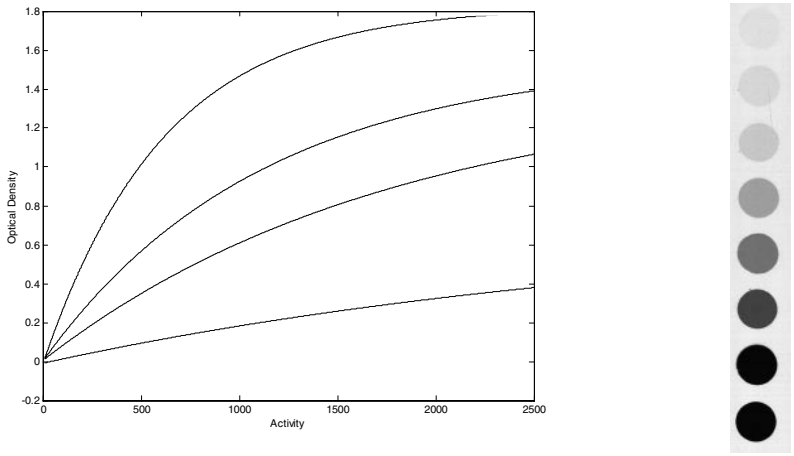

a *b*

Figure 3-3. *a) Optical densities of ^{14}C-PMMA calibration sources of different exposure times:1, 2, 5 and 15 days exposed on Kodak Biomax MR autoradiography film – scanned with Ricoh FS2 flatbed scanner using 300 dpi resolution. b) An autoradiograph of the calibration sources exposed during 5 days.*

Resolution

The radiographic image of a point is not a point, but it is made up from developed silverhalogenide crystals located at different distances from the source. Figure 3-4 shows a backscattered electron image of the PMMA impregnated rock sample and the corresponding autoradiograph digitized by CCD camera (Hamamatsu). The figure illustrates the spatial resolution of the autoradiography method. The porous minerals form even grey areas on the autoradiograph.

The energy of the used radioactive nuclide has a high impact on the resolution. It influences the range in the rock as well as the absorption of the beta particles on the autoradiography film emulsion layer. Other important factors for the resolution are the distance between the autoradiography film and the rock source and the quality of the rock surfaces.

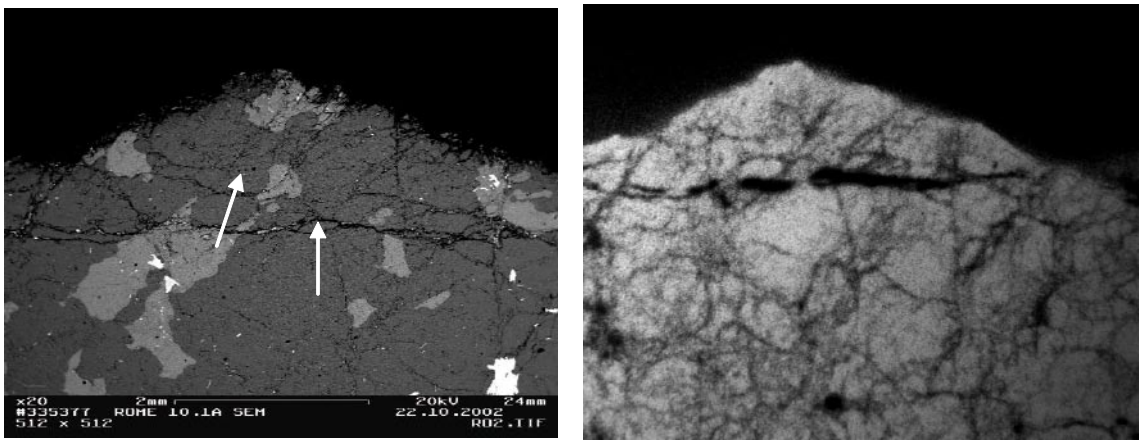

a *b*

Figure 3-4. *Backscattered electron image (a) and corresponding autoradiograph (b) of a PMMA impregnated rock sample illustrating resolution characteristics of the method.*

3.3.4 Digital image analysis of ^{14}C-PMMA autoradiographs

Interpretation of the results is based on digital image analysis of the autoradiograph. Digital image analysis started by dividing the autoradiograph into area units called pixels. The rock surfaces and the film autoradiographs were digitized with a Canon 9900 table scanner using 1,200 dpi resolution. In this study, the 600 dpi resolution was used in the quantitative analysis. Essentially, all the intensities of the sub-domains were converted into corresponding optical densities, and these were in turn converted into levels of activity with the help of the calibration curves measured for each exposure. Finally, the levels of activity were converted into their corresponding porosities. In principle, the interpretation is based on studying the abundance of tracer in each sub-domain. Reference /1/ contains the basic calculations related to porosity determination. The software program Mankeli for quantitative porosity measurement was used in this study, implemented using the Matlab Image Processing Toolbox.

Calculation of porosity

Intensity and optical density

Since the response of the image source (a flatbed scanner) and the amplifier of the digital image analyser are linear, the digitised grey levels of the film can be treated as intensities. Optical densities, which according to Lambert & Beer's law are proportional to concentration, are derived from the intensities:

$$D = -\log\left(\frac{I}{I_0}\right) \qquad 3\text{-}1$$

where D is the optical density, I0 is the intensity of the background and I is the intensity of the sample. It can be seen that as the intensity decreases, the optical density increases.

Activity and optical density

A conversation function is required to relate the measured optical densities to the corresponding levels of activity. ^{14}C-PMMA standards (tracer diluted with inactive MMA) having specific activities between 462 and 185,000 Bq/ml were used to establish the calibration function. The construction of the calibration curves which enable the quantitative measurement of the autoradiograph obtained by the PMMA method is conducted by an iterative calculation of three parameters (a,k,c). For a given exposure time the mathematical function describing the nonlinear behaviour of the local activity versus optical density of the film has the principle form:

$$D = a\left(1 - e^{-kA}\right) + c \qquad 3\text{-}2$$

where D is the optical density and A is the specific activity. The equation is written in the form:

$$\ln\left(A_b - D\right) = -kA + C \qquad 3\text{-}3$$

where the parameters A_b= a+c = D_{max}, k and C= ln(a) = D_0 are found iteratively by the least squares method (first the value of A is iterated to give the best correlation with the data points and then k and C are calculated) and the activity in the rock sample is calculated from the measured optical density. Solving A from above equation gives:

$$A = \frac{\ln(D_{\max} - D) - D_0}{-k} \qquad 3\text{-}4$$

Porosity

The local porosity ε of the sample was simply obtained from the abundance of the tracer (assuming that the concentration of tracer in the PMMA is constant, the higher the abundance of the tracer, the higher the local porosity):

$$\varepsilon = \beta(A / A_0) \times 100 \qquad 3\text{-}5$$

where A_0 is the specific activity of the tracer used to impregnate the rock matrix, and β is the β-absorption correction factor. The absorption of β radiation in a substance depends on the density of the substance in a roughly linear fashion. The factor β can therefore be approximated from:

$$\beta = \rho_s / \rho_0 \qquad 3\text{-}6$$

where ρ_s is the density of the sample and ρ0 is the density of pure PMMA (1.18 g/cm^3). In this interpretation, the sample is assumed to consist of rock material and pores (containing PMMA). ρs can therefore be expressed as:

$$\rho_s = \varepsilon\rho_0 + (1-\varepsilon)\rho_r \qquad 3\text{-}7$$

where ρ_r is the density of the mineral grains. In bulk measurements the average density of the rock sample is used instead of mineral density. Using Equations 4-6 and 4-7 in Equation 3-5, the porosity and the activity relationship can be solved:

$$\varepsilon = \frac{\frac{\rho_r}{\rho_0}}{1+\left(\frac{\rho_r}{\rho_0}-1\right)\frac{A}{A_0}}\frac{A}{A_0} \qquad 3\text{-}8$$

where A is the specific activity of an individual pixel and A_0 is the specific activity of the tracer. The porosity of each individual pixel n from the autoradiogram is calculated according to Equations 3-4 and 3-8. The porosity histogram provides the relative frequency of regions of different individual porosities. The total PMMA porosity is obtained from the porosity distribution by taking a weighted average:

$$\varepsilon_{tot} = \frac{\sum_n Area_n \varepsilon_n}{\sum_n Area_n} \qquad 3\text{-}9$$

where $Area_n$ is the area of pixel n, and εn is the local porosity of pixel n.

The amount of tracer in the sample, and the volumetric porosity, can therefore be derived from the blackening of the film caused by the radiation emitted from the plane surface of the rock section. Figure 3-5 shows an example of the autoradiograph and the porosity distribution of sample F4. If the pore sizes are well below the resolution of the autoradiography, the major fraction of the beta radiation emitted is attenuated by silicate. The tracer can thus be considered to be diluted by silicate. For the ^{14}C-PMMA method to be used, the bulk density must be known, there must be only two phases (i.e. mineral and PMMA), and the pores and minerals must be homogeneously distributed below the lateral resolution limit of the autoradiography.

Porosity profiles were measured from the autoradiograph if the sample was taken adjacent to a water bearing fracture and the porosity pattern showed any changes according to the distance from the surface. Figure 3-6 shows a profile measurement example measured from the autoradiograph of sample F8.

3.4 Digital autoradiography with FLA-5100

The new FujiFilm FLA-5100 imaging system allows imaging of fluorescent and radioisotopic samples. Imaging plates are flexible image sensors in which bunches of very small crystals of photo-stimulable phosphorus barium fluorobromide containing a trace amount of bivalent

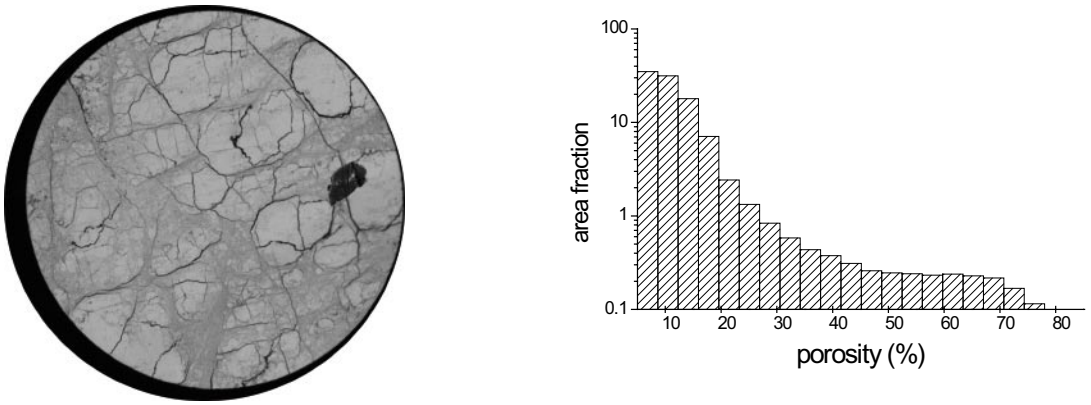

a *b*

Figure 3-5. *a) Autoradiograph of sample F4 and b) corresponding porosity histogram. A total PMMA porosity of 7.5% was determined. Sample diameter is c.51 mm.*

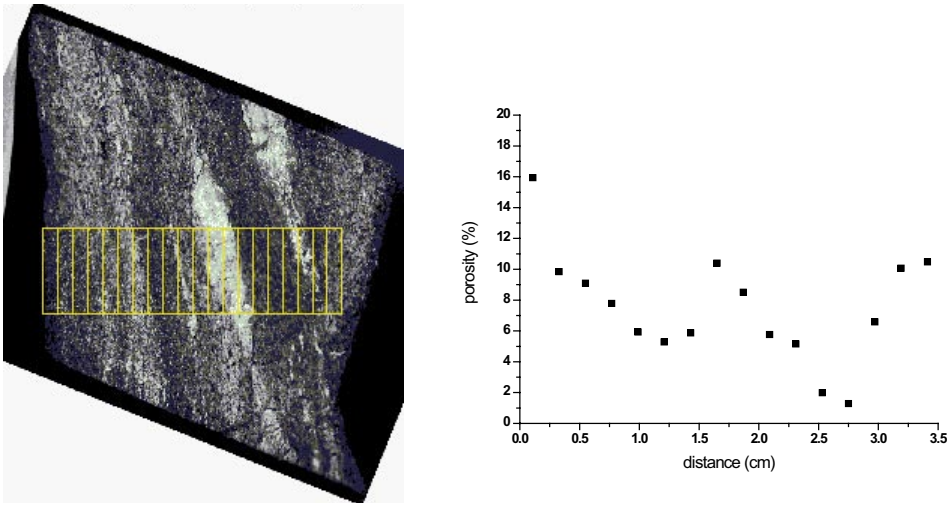

a *b*

Figure 3-6. *a) Autoradiograph of sample F8. Fracture surface is on the left of this image. Sample width is 4 cm.* ***b)*** *Porosity profile measured from the autoradiograph.*

europium as a luminescence center, formulated as BaFBr:Eu2+, are uniformly coated on a polyester support film. Exposure of samples on an imaging plate is similar to that of photo-film but it can be re-used after erasing the latent image from the plate with uniform white light.

The area of linearity achieved with the FLA-5100 scanner is five orders of magnitude, when the linear area in film autoradiograhy is only two orders of magnitude. The IPs are 50–100 times more sensitive than film autoradiography films. This allows shorter exposure times and a better separation power when using samples with high energy nuclides.

This study provided an excellent opportunity for HYRL to compare the two different imaging methods: film autoradiography and digital autoradiography. All the samples have been imaged with both methods, but the quantitative porosity analysis has been done from film autoradiographs. The images achieved with the FLA-5100 scanner are presented in this report as colour images in next chapter.

3.5 Nonconformities

There are no nonconformities with respect to the activity plan or the method description.

4 Results of PMMA analyses

4.1 Sample F1 (KFM01A)

The photograph taken of sample F1, before any operation, and the partition diagram are presented in Appendix 1. A photo image of the analysed rock surface is presented below in Figure 4-1a and the corresponding film and digital autoradiographs are shown in Figures 4-1b and 4-1c, respectively. The exposure time on the film autoradiograph has been 21 days and on the digital autoradiograph 3 days.

The PMMA porosity of sample F1 was 0.1%. The rock represents medium grained granite changing to granodiorite, the matrix was metamorphic. The rock sample has been fully impregnated, intragranular porosity dominates. The porosity distribution is even; grain boundary porosity was not found, indicating low permeability matrix. Figure 4-2 shows the porosity histogram for sample F1 achieved with the PMMA method. The water gravimetry porosities, measured at HYRL and given by SKB (Eva Gustavsson, Geosigma) for sample F1 were 0.15% and 0.19%, respectively.

a *b* *c*

Figure 4-1. *a) the analysed rock surface of sample F1, b) its corresponding film autoradiograph and c) its corresponding digital autoradiograph.*

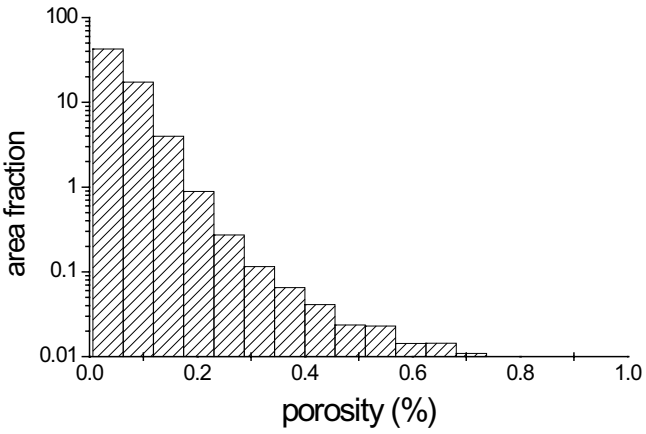

Figure 4-2. *Porosity histogram of sample F1. A total PMMA porosity of 0.1% was determined.*

4.2 Sample F2 (KFM02A)

The photograph taken of sample F2, before any operation, and the partition diagram are presented in Appendix 2. Two samples of F2 were impregnated. The photo image of the rock surface of the first sample, F2A, is presented below in Figure 4-3a and the corresponding film and digital autoradiographs are shown in Figures 4-3b and 4-3c, respectively. In Figure 4-4a the rock surface photo image of the second sample, F2B, is presented and the corresponding film and digital autoradiographs are shown in Figures 4-4b and 4-4c, respectively. The second sample was irradiated in ^{14}C-MMA due to the high porosity and high permeability of the sample. For both samples the exposure time on the film autoradiograph has been 7 days and on the digital autoradiograph 1 day.

Figure 4-3 shows the first improper PMMA impregnation result; holes inside the matrix are empty due to the out diffusion of tracer. To avoid any out diffusion of the intruded MMA during the polymerisation step, a second F2 sample was impregnated and irradiated in the tracer.

The PMMA porosity measured for sample F2B was 10%. Rock sample F2 represents a medium-grained granite to granodiorite which has been exposed to episyenitisation. The rock sample was fully impregnated and visible holes were found in the matrix filled with pure PMMA. These areas were excluded from the quantitative porosity measurement, because the pure PMMA areas do not fulfill the conditions for PMMA porosity measurement. Figure 4-5 shows the porosity histogram for the sample F2B. From the autoradiograph is was found a heterogeneous porosity distribution containing low porous ground matrix, highly to moderately porous mineral patches, and the last phases are the open pores filled with the PMMA. Porous mineral grains showed 20–30% porosity. The water gravimetry porosities, measured at HYRL and given by SKB (Eva Gustavsson, Geosigma), for sample F2 were 11.5% and 16%, respectively.

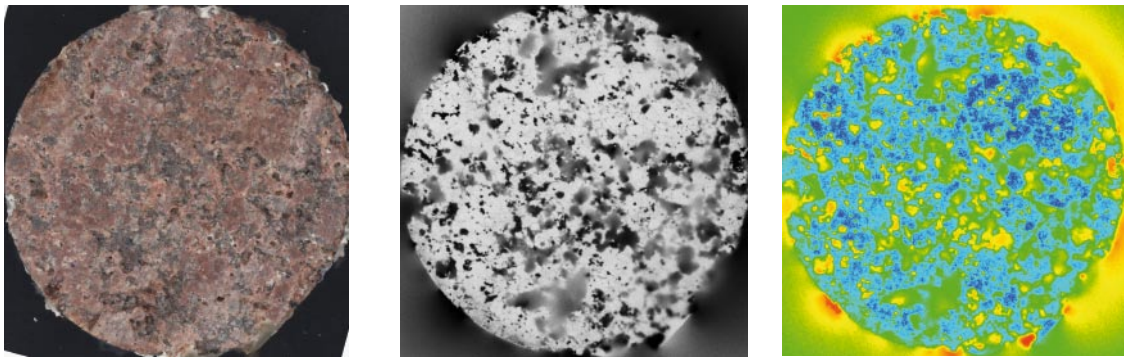

a *b* *c*

Figure 4-3. *a) the analysed rock surface of sample F2A, b) its corresponding film autoradiograph and c) its corresponding digital autoradiograph.*

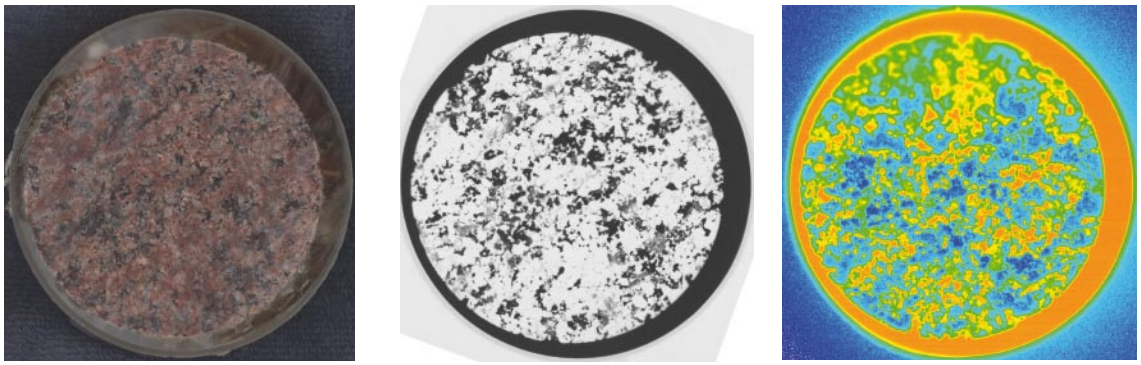

a *b* *c*

Figure 4-4. *a) the analysed rock surface of sample F2B, b) its corresponding film autoradiograph and c) its corresponding digital autoradiograph.*

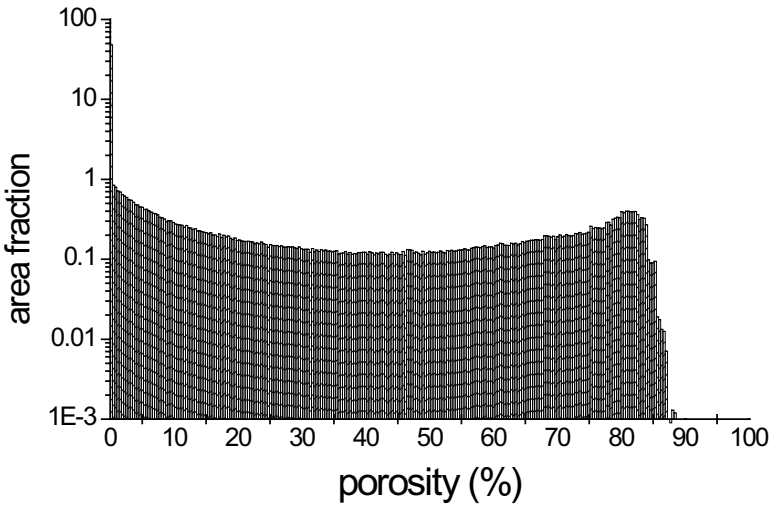

Figure 4-5. *Porosity histogram of sample F2B. A total PMMA porosity of about 10% was determined.*

4.3 Sample F3 (KFM02A)

The photograph taken of sample F3, before any operation, and the partition diagram are presented in Appendix 3. A photo image of the analysed rock surface after impregnation and sawing is presented below in Figure 4-6a and the corresponding film and digital autoradiographs are shown in Figures 4-6b and 4-6c, respectively. The exposure time on the film autoradiograph has been 21 days and on the digital autoradiograph 3 days.

The PMMA porosity of the sample F3 was 0.05%. The rock sample has been fully impregnated, grain boundary porosity dominates. The rock represents fine- to medium- grained granite changing to granodiorite and tonalite, the matrix was metamorphic. Figure 4-7 shows the porosity histogram for sample F3 achieved with the PMMA method. The water gravimetry porosities, measured at HYRL and given by SKB (Eva Gustavsson, Geosigma), for sample F3 were 0.2% and 0.28%, respectively.

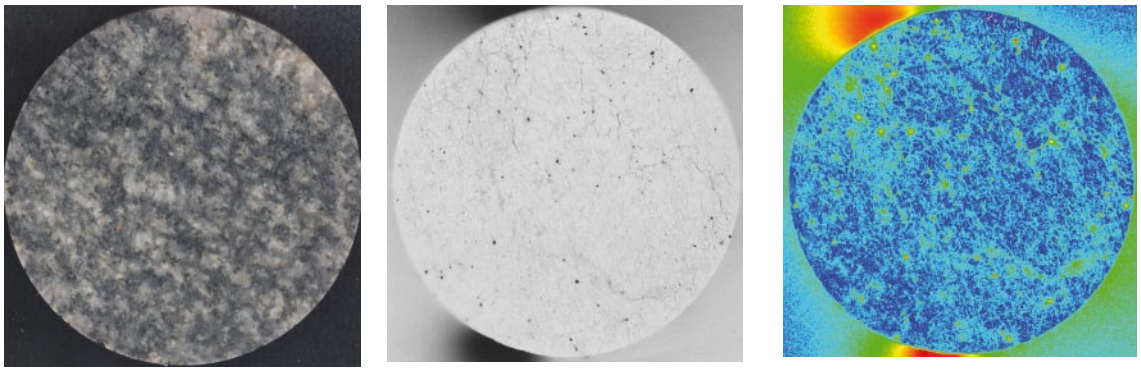

a *b* *c*

Figure 4-6. *a) the analysed rock surface, b) its corresponding film autoradiograph and c) its corresponding digital autoradiograph.*

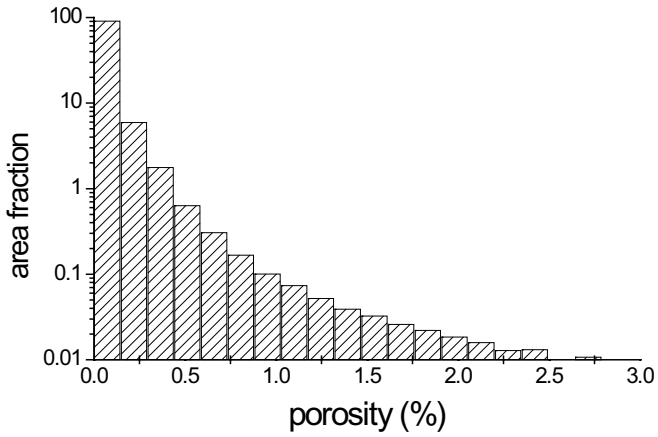

Figure 4-7. *Porosity histogram of sample F3. A total PMMA porosity 0.05% was determined.*

4.4 Sample F4 (KFM04A)

The photograph taken of sample F4, before any operation, and the partition diagram are presented in Appendix 4. Two samples of F4 were impregnated. The photo image of the rock surface of sample F4A after impregnation and sawing is presented below in Figure 4-8a and the corresponding film and digital autoradiographs are shown in Figures 4-8b and 4-8c, respectively. In Figure 4-9a the rock surface photo image of sample F4B is presented and the corresponding film and digital autoradiographs are shown in Figures 4-9b and 4-9c, respectively. The second sample was irradiated in ^{14}C-MMA due to the high porosity and high permeability of this sample. For both samples the exposure time on the film autoradiograph was 7 days and on the digital autoradiograph 1 day.

Figure 4-8 shows an improper PMMA impregnation result; holes inside the matrix are empty due to the out diffusion of tracer. To avoid any out diffusion of the intruded MMA during the polymerisation step, a second F4 sample was impregnated and irradiated in the tracer.

The PMMA porosity for sample F4B was 7.5%, which corresponds well to the water gravimetry result of 7.9% measured at HYRL. The rock sample has been fully impregnated, intra granular porosity in altered clayish phases can be seen. The porosity pattern of this sample shows a heterogeneous structure. Grain boundaries of mineral phases are highly porous or open, strongly altered clayish matrix shows intragranular even porosity pattern and dark red coloured mineral phases display a low PMMA porosity. Figure 4-10 shows the porosity histogram for sample F4B achieved with the PMMA method. Figure 4-11 presents the autoradiogram of F4B with porosity of over 10% in red colour.

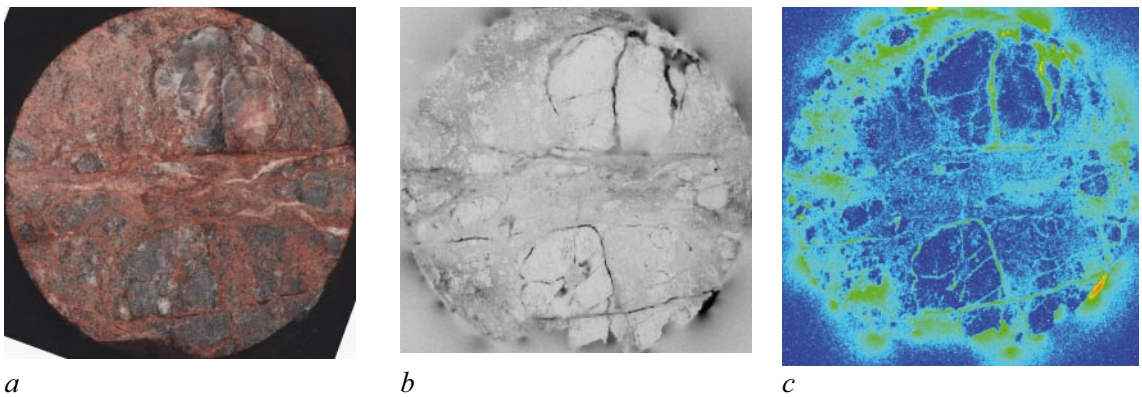

a *b* *c*

Figure 4-8. *a) the analysed rock surface of sample F4A, b) its corresponding film autoradiograph and c) its corresponding digital autoradiograph.*

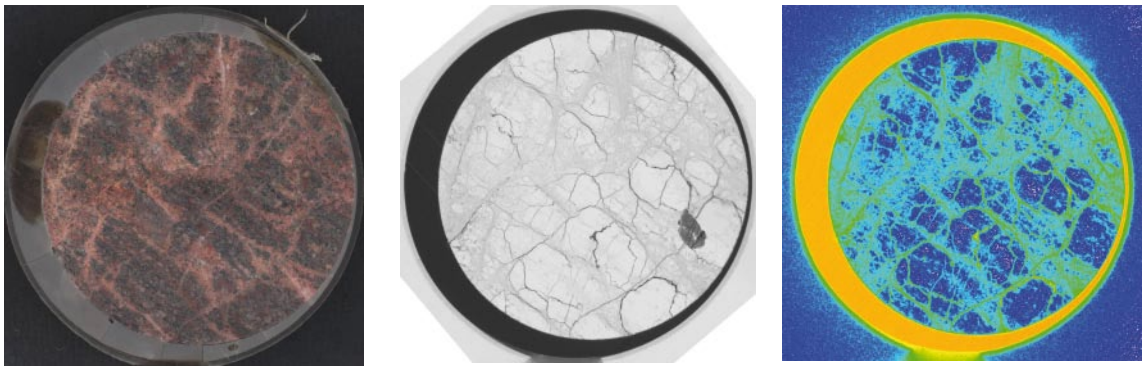

a *b* *c*

Figure 4-9. *a) the analysed rock surface, b) its corresponding film autoradiograph and c) its corresponding digital autoradiograph.*

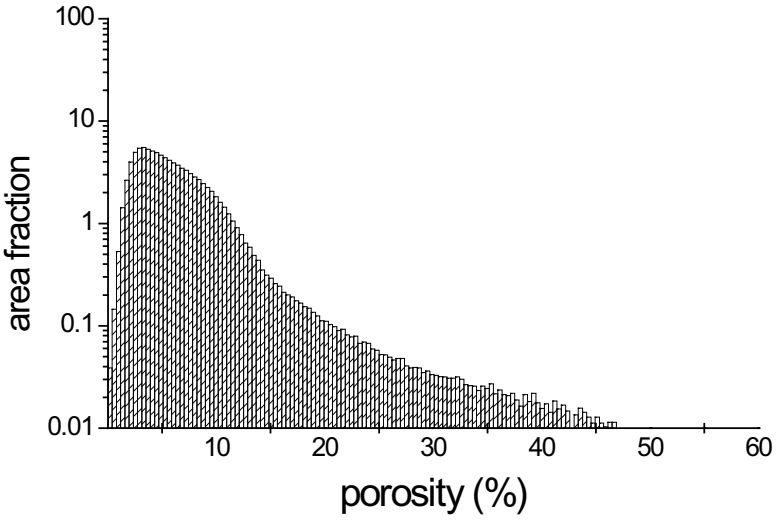

Figure 4-10. *Porosity histogram of sample F4. A total PMMA porosity of about 7.5% was determined.*

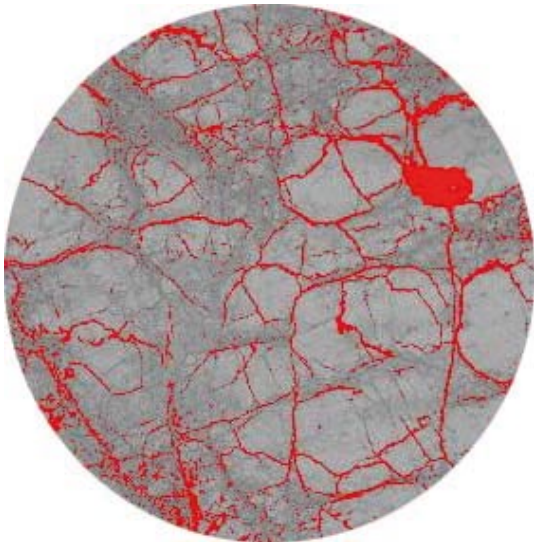

Figure 4-11. *Autoradiograph of sample F4B with a porosity of over 10% shown in red.*

4.5 Sample F5 (KFM05A)

The photograph taken of sample F5, before any operation, and the partition diagram are presented in Appendix 5. After impregnation the sample was sawn in two pieces. The photo images of the analysed rock surfaces after impregnation and sawing for samples F5A and F5B are presented below in Figures 4-12a and 4-13a. The corresponding film and digital autoradiographs for sample F5A are shown in Figures 4-12b and 4-12c, and for sample F5B in Figures 4-13b and 4-13c, respectively. For both samples the exposure time on the film autoradiograph was 21 days and on the digital autoradiograph 3 days.

The total PMMA porosity for the F5 sample is 0.05%. MMA has intruded improperly into the rock matrix. The rock type was granite, metamorphic, and the texture was fine- to medium-grained. A few micro fissures transecting the sample are visualized, the grain boundary porosity dominates. A few mafic mineral grains are porous close to the fracture surface in the F5B sample sawn parallel to the core axis. Figure 4-14 shows the porosity histogram for sample F5A, sawn perpendicular to the core axis, achieved with the PMMA method. A few micro fissures transect the sample, the grain boundary porosity dominates. Most minerals are none porous by PMMA technique. Water gravimetry porosity measured at HYRL was 0.2%.

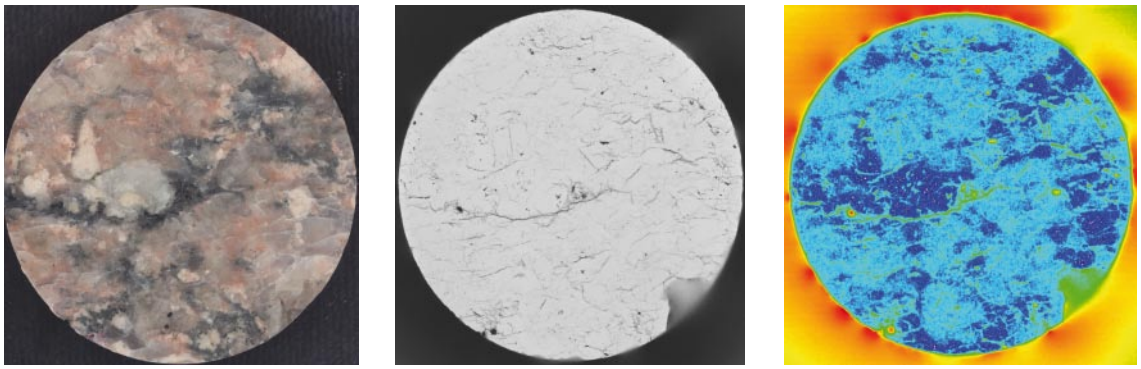

a *b* *c*

Figure 4-12. *a) the analysed rock surface of sample F5A, b) its corresponding film autoradiograph and c) its corresponding digital autoradiograph.*

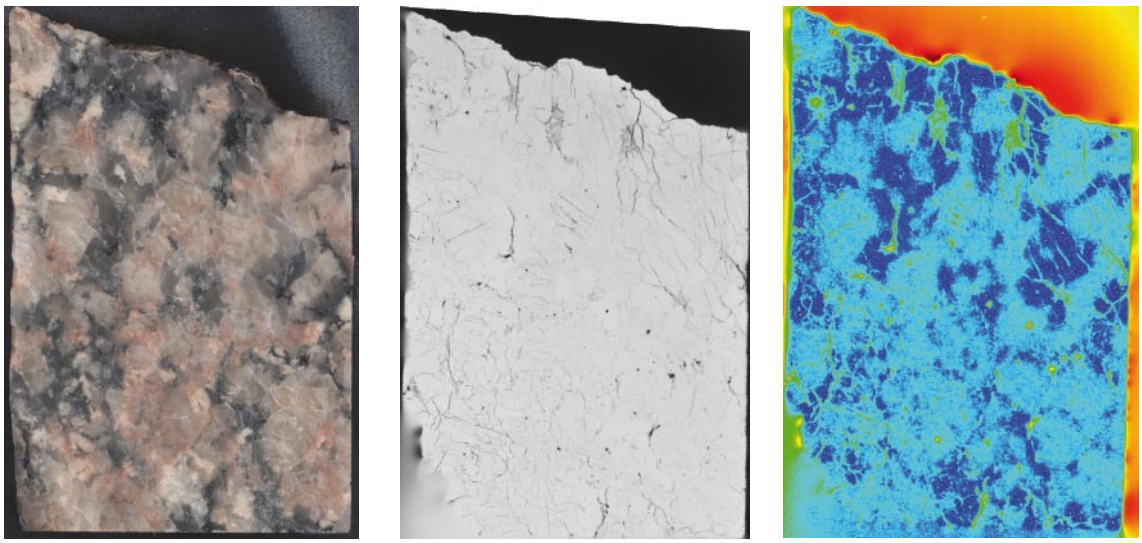

a *b* *c*

Figure 4-13. *a) the analysed rock surface of sample F5B, b) its corresponding film autoradiograph and c) its corresponding digital autoradiograph.*

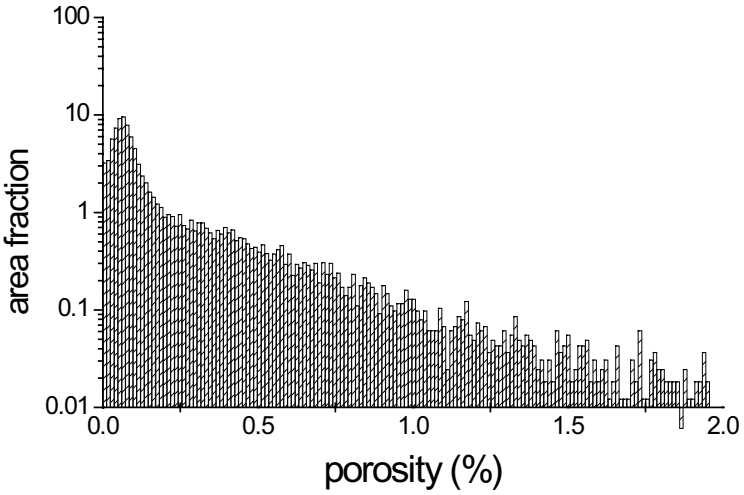

Figure 4-14. *Porosity histogram of sample F5A. A total PMMA porosity of about 0.05% was determined.*

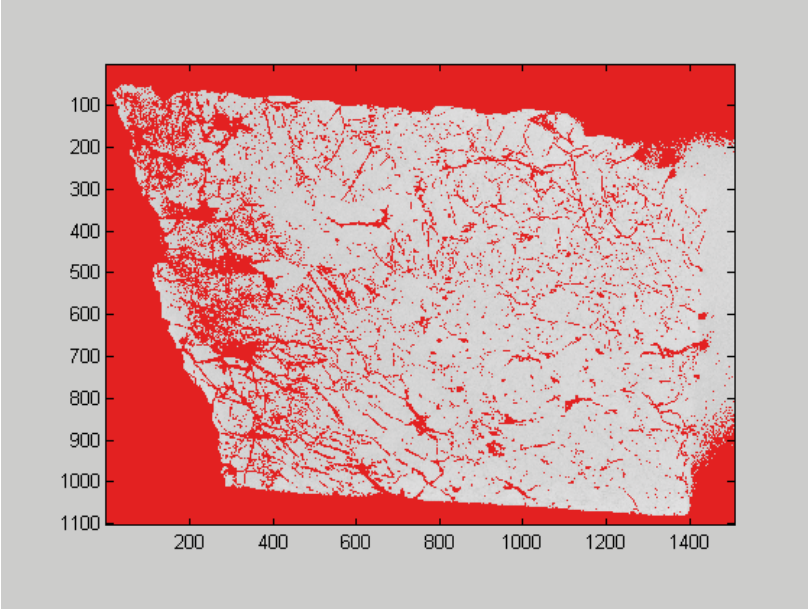

Figure 4-15. *Autoradiograph of sample F5B with porosity of over 0.2% shown in red.*

4.6 Sample F6 (KFM03A)

The photograph taken of sample F6, before any operation, and the partition diagram are presented in Appendix 6. A photo image of the analysed rock surface after impregnation and sawing is presented below in Figure 4-16a and the corresponding film and digital autoradiographs are shown in Figures 4-16b and 4-16c, respectively. The exposure time on the film autoradiograph was 25 days and on the digital autoradiograph 4 days.

The PMMA porosity for the F6 sample is 0.1%. Figure 4-17 shows the porosity histogram for F6 achieved with the PMMA method. The rock sample has been fully impregnated; slight foliation can be seen on the autoradiograph visualising the porosity pattern of this sample, not following the texture of minerals. With water gravimetry the porosity for sample F6 was 0.2%. In Figure 4-18 a porosity of over 0.25% is shown in red colour.

a *b* *c*

Figure 4-16. *a) the analysed rock surface of sample F6, b) its corresponding film autoradiograph and c) its corresponding digital autoradiograph.*

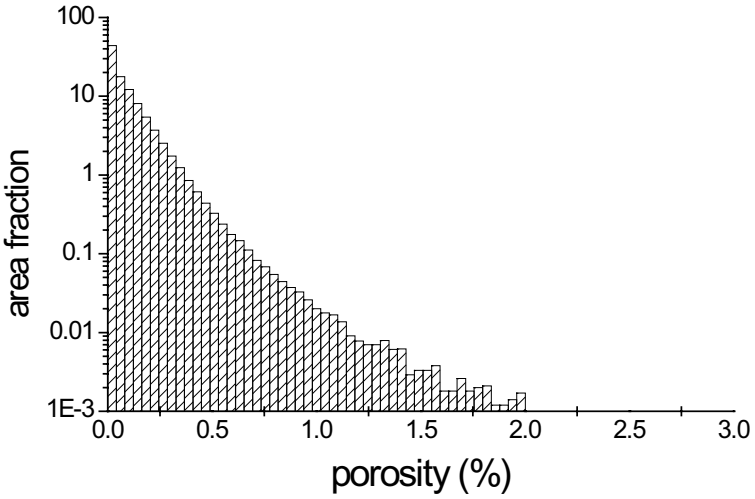

Figure 4-17. *Porosity histogram of sample F6. A total PMMA porosity of about 0.1% was determined.*

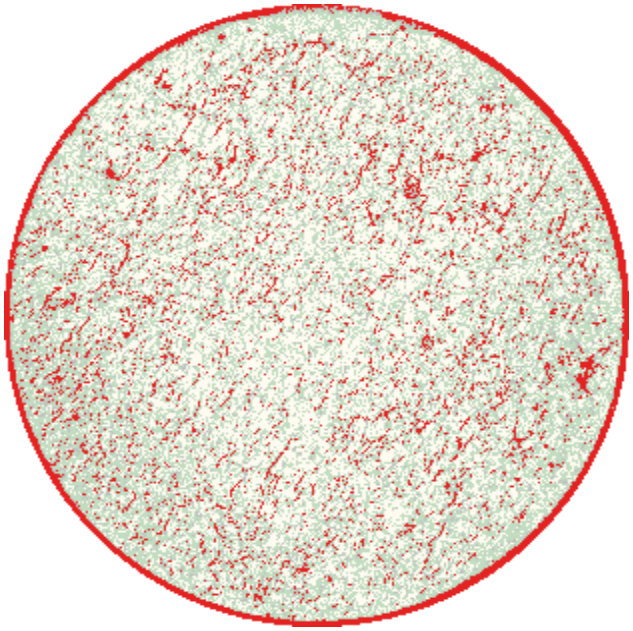

Figure 4-18. *Autoradiograph of sample F6 with a porosity of over 0.25% shown in red.*

4.7 Sample F7 (KFM04A)

The photograph taken of sample F7, before any operation, and the partition diagram are presented in Appendix 7. A photo image of the analysed rock surface after impregnation and sawing is presented below in Figure 4-19a and the corresponding film and digital autoradiographs are shown in Figures 4-19b and 4-19c, respectively. The exposure time on the film autoradiograph was 14 days and on the digital autoradiograph 4 days.

The PMMA porosity of the low porous area of sample F7 was 0.5% and the altered mineral phases showed higher porosities; 4%. Figures 4-20b and 4-21b display the porosity histograms for F7 achieved with the PMMA method from the areas indicated in Figures 4-20a and 4-21a, respectively. The rock sample is fully impregnated. The porosity pattern follows the schistosity of the mineral texture. Minerals with a porosity of over 5% seem to be chloritized biotite. A few porous veins or tiny fractures cutting the sample perpendicular to the foliation are seen clearly on the autoradiograph. In Figures 4-22a and 4-22b porosities of over 1 and 5% are shown in red colour, respectively.

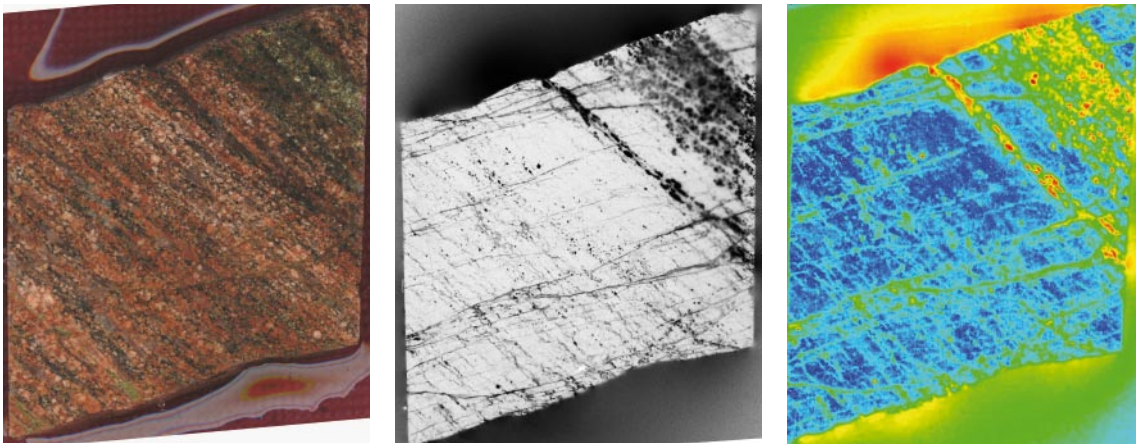

a *b* *c*

Figure 4-19. *a) the analysed rock surface of sample F7, b) its corresponding film autoradiograph and c) its corresponding digital autoradiograph.*

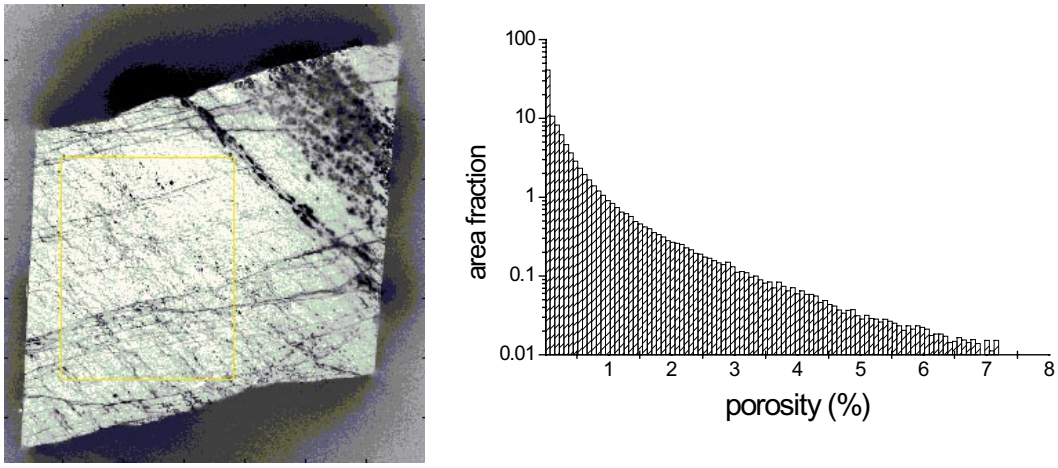

a *b*

Figure 4-20. *Porosity histogram of sample F7. A total PMMA porosity of 0.5% was determined.*

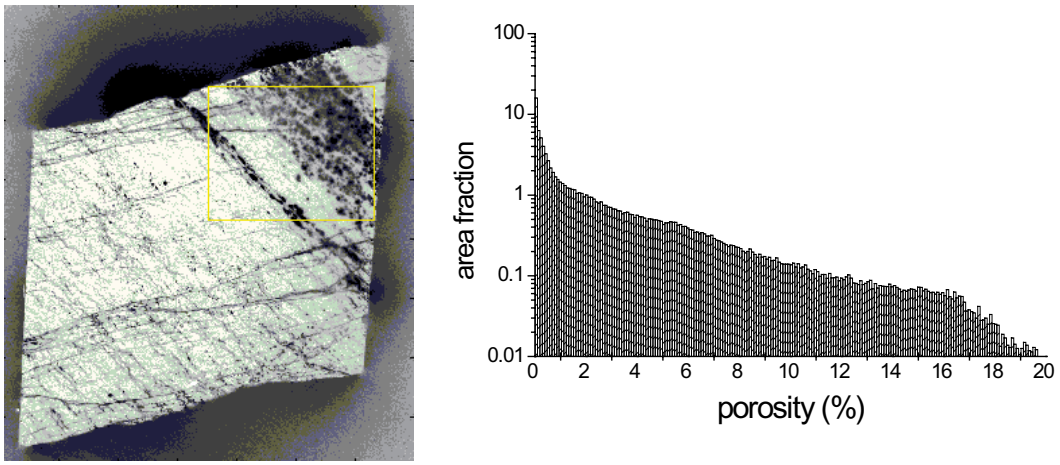

a *b*

Figure 4-21. *Porosity histogram of sample F7. A total PMMA porosity of about 4% was determined.*

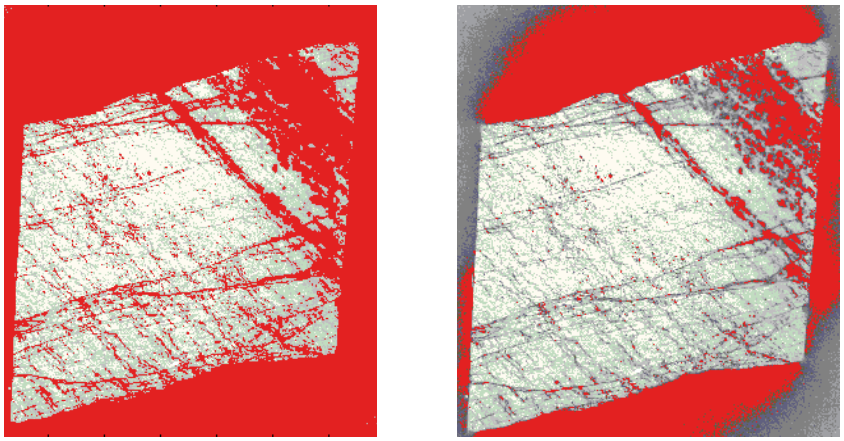

a *b*

Figure 4-22. *Autoradiographs of sample F7 where a) a porosity of over 1% is shown in red and b) a porosity of over 5% is shown in red.*

4.8 Sample F8 (KFM04A)

The photograph taken of sample F8, before any operation, and the partition diagram are presented in Appendix 8. Sample F8 came in two pieces, which were impregnated and analysed separately. The photo images of the analysed rock surfaces after impregnation and sawing for samples F8A and F8B are presented below in Figures 4-23a and 4-24a. The corresponding film and digital autoradiographs for sample F8A are shown in Figures 4-23b and 4-23c, and for sample F8B in Figures 4-24b and 4-24c, respectively. The exposure time on the film autoradiograph was 4 days and on the digital autoradiograph 1 hour for both samples.

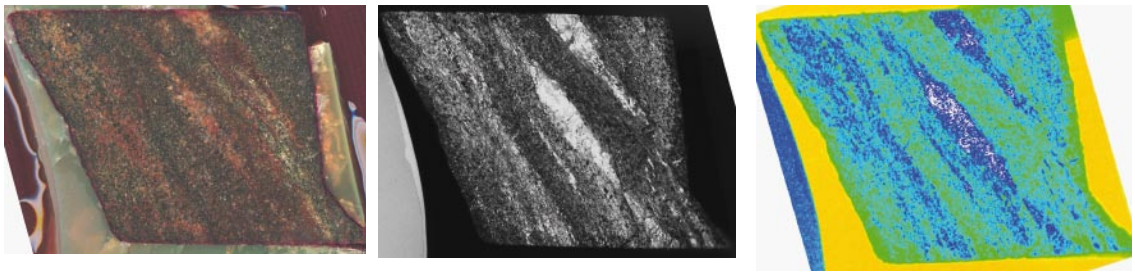

a *b* *c*

Figure 4-23. *a) the analysed rock surface of sample F8A, b) its corresponding film autoradiograph and c) its corresponding digital autoradiograph.*

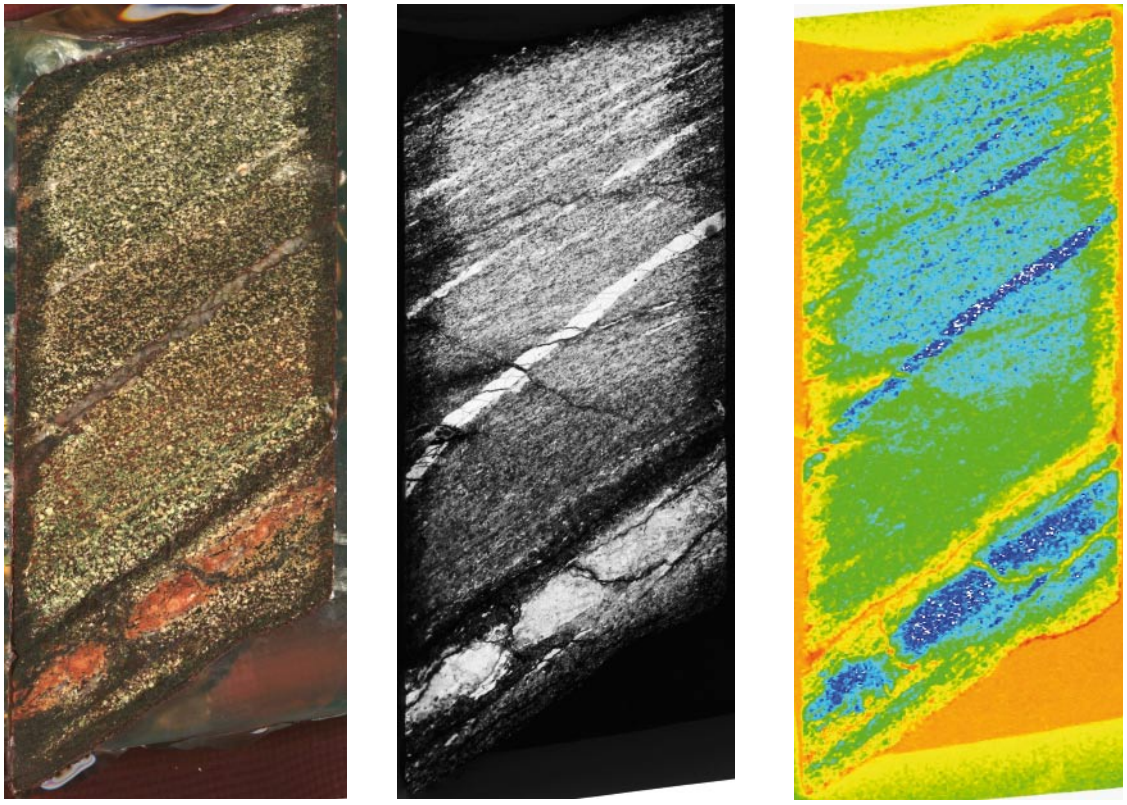

a *b* *c*

Figure 4-24. *a) the analysed rock surface of sample F8B, b) its corresponding film autoradiograph and c) its corresponding digital autoradiograph.*

The PMMA porosity of sample F8A was 7%. Figure 4-25 shows the porosity histogram for F8A achieved with the PMMA method. The PMMA porosity of sample F8B varied between 5 and 12%. The rock sample has been fully impregnated. This sample is taken close to a water bearing fracture and the rock is highly porous to a depth of centimetres. Mineral grains with up to 20% porosity have been detected. The structure shows a foliation congruent with the mineral texture. Mineral grains of low porosity are observed in the matrix. This sample was irradiated under initial tracer ^{14}C-MMA solution and the structure kept its shape during the polymerisation step. A porosity profile from the sample F8A was measured to a depth of 4 cm from the fracture surface as shown in the Figure 4-26. A porosity profile from the sample F8B was measured to a depth of 3 cm from the fracture surface as shown in Figure 4-27.

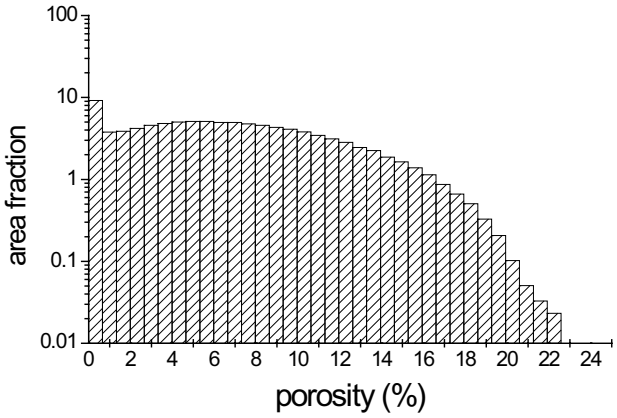

Figure 4-25. *Porosity histogram of sample F8A. A total PMMA porosity of 7% was determined.*

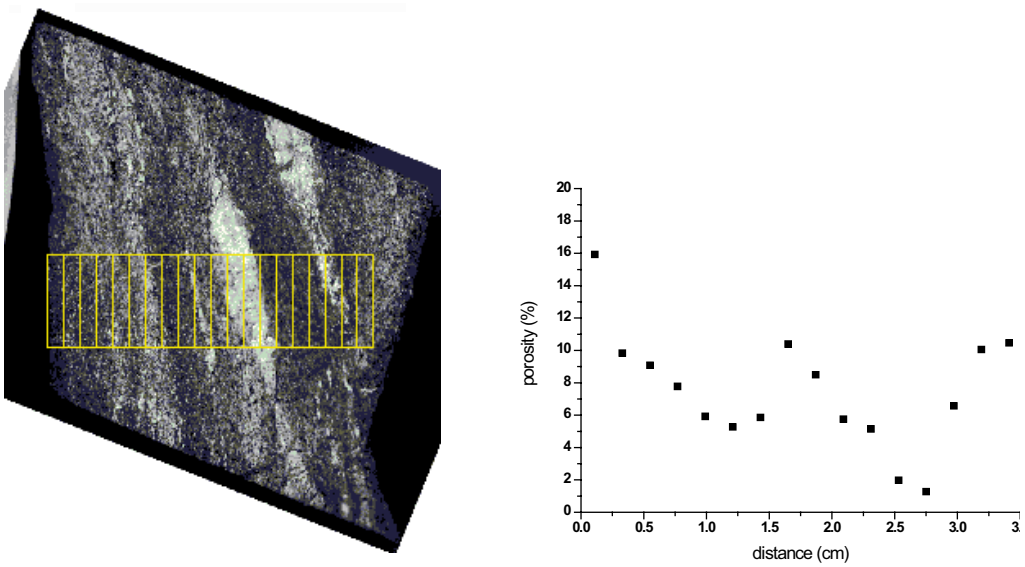

a *b*

Figure 4-26. *a) the regions on the autoradiograph used in the porosity profile measurement and b) the porosity profile for sample F8A.*

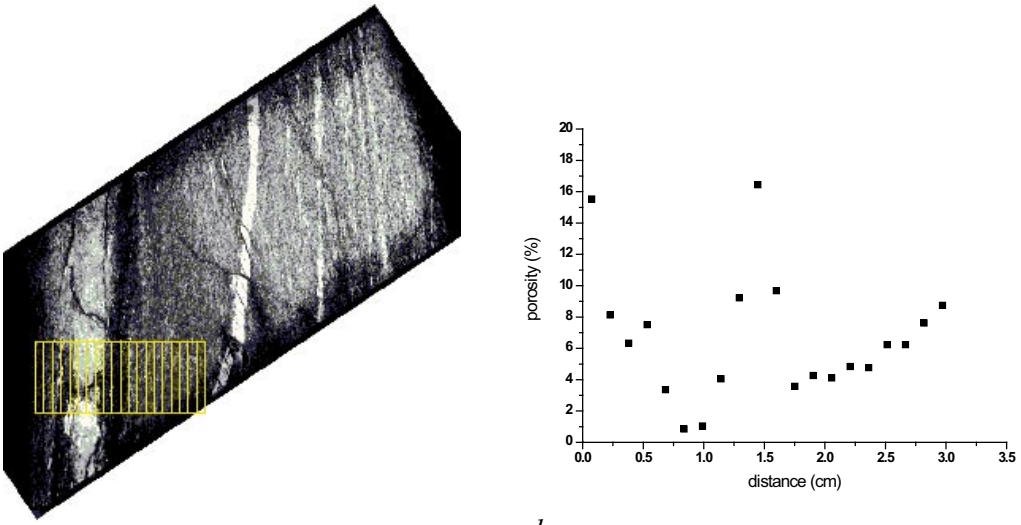

a *b*

Figure 4-27. *a) the regions on the autoradiograph used in the porosity profile measurement and b) the porosity profile for sample F8B.*

4.9 Sample F9 (KFM05A)

The photograph taken of sample F9, before any operation, and the partition diagram are presented in Appendix 9. A photo image of the analysed rock surface after impregnation and sawing is presented below in Figure 4-28a and the corresponding film and digital autoradiographs are shown in Figures 4-28b and 4-28c, respectively. The exposure time on the film autoradiograph was 7 days and on the digital autoradiograph 23 hours.

Sample F9 is partly highly porous. This sample represents a laumontite type breccia. Laumontite is one type of zeolites, which are normally difficult to dry and impregnate without any changes during the PMMA procedure. The whole rock was fully impregnated with ^{14}C-MMA. During irradiation polymerisation step, highly porous phases were broken due to PMMA shrinkage. Total PMMA porosity is 3% in the low porosity phases (Figure 4-29), but up to 50% porosities were measured in some areas. The sample consists of rock grains with large grain sizes; from 0.5 to 2 cm in diameter. These large grains are slightly porous. The grain boundaries are open; PMMA rings around the rock grains were found. The ground matrix (clayish type) between the grains show either a porosity of a few percents or is highly (> 30%) porous.

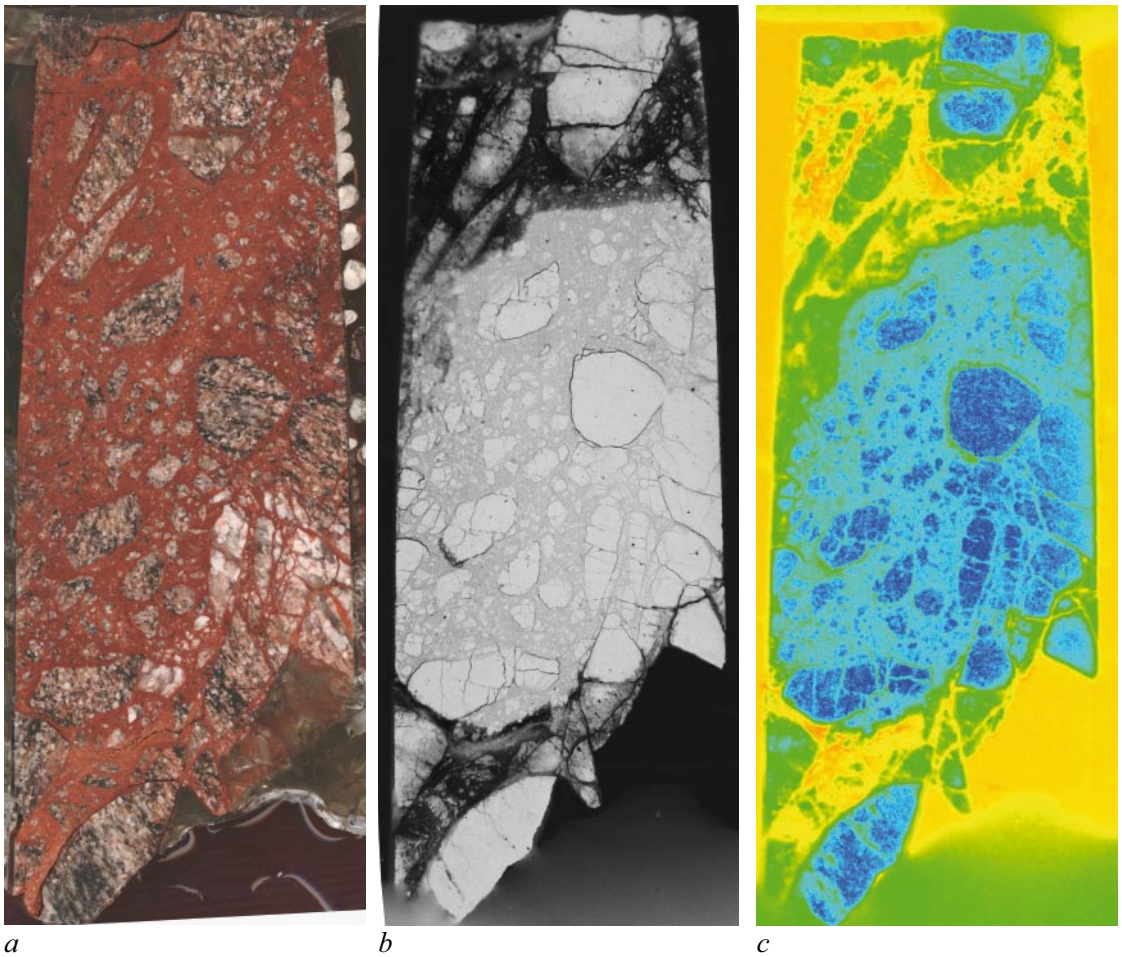

a *b* *c*

Figure 4-28. *a) the analysed rock surface of sample F9, b) its corresponding film autoradiograph and c) its corresponding digital autoradiograph.*

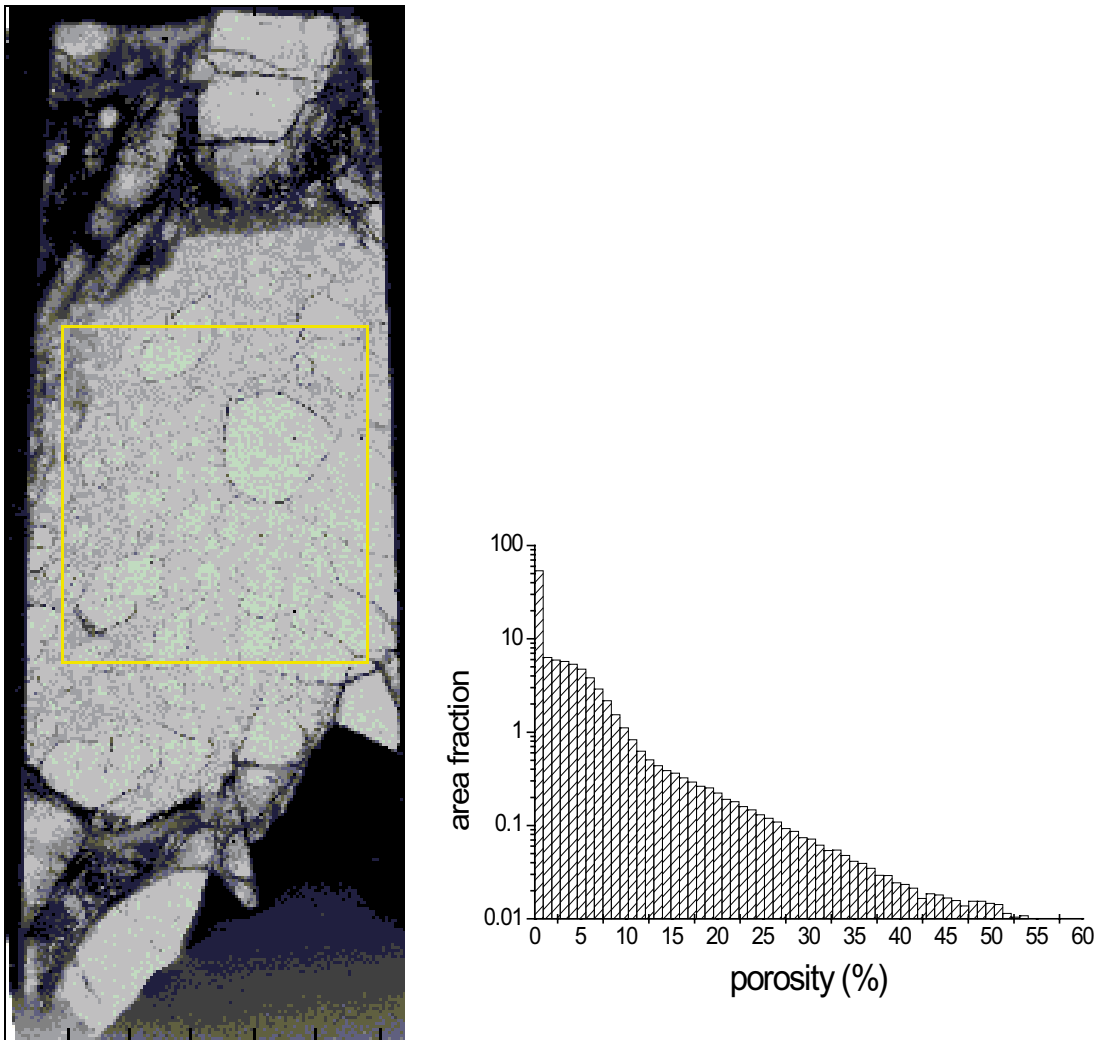

Figure 4-29. *Porosity histogram of sample F9. A total PMMA porosity of 3% was determined.*

4.10 Sample F10 (KFM05A)

The photograph taken of sample F10, before any operation, and the partition diagram are presented in Appendix 10. After impregnation the sample was sawn in two pieces. The photo images of the analysed rock surfaces after impregnation and sawing are presented below in Figures 4-30a and 4-31a, the corresponding film and digital autoradiographs for sample F10A are shown in Figures 4-30b and 4-30c, and for sample F10B in Figures 4-31b and 4-31c, respectively. The exposure time on the film autoradiograph was 20 days and on the digital autoradiograph 2 days.

The PMMA porosity of the sample F10 was ≤ 0.1%. Figure 4-32 shows the porosity histogram for F10B achieved with the PMMA method. The samples have not been fully impregnated. In regions where PMMA can be seen on the autoradiograph, the grain boundaries have been slightly visualised. Very low porosity is measured for both samples indicating very tight matrix and low permeability. Only the surroundings of a fissure transecting the sample F10B show higher porosity that can be visualised.

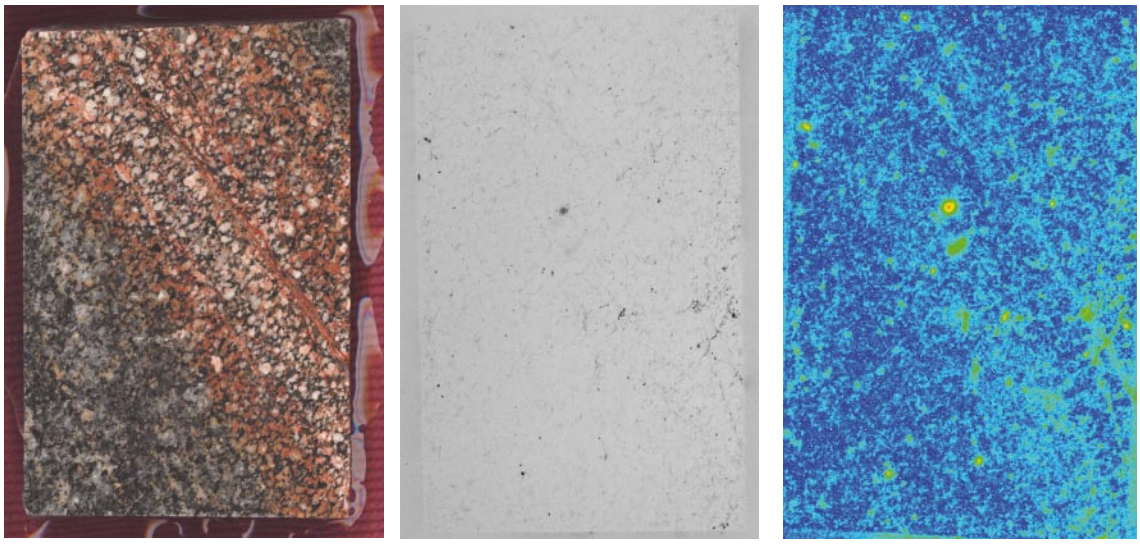

a *b* *c*

Figure 4-30. *a) the analysed rock surface of sample F10A, b) its corresponding film autoradiograph and c) its corresponding digital autoradiograph.*

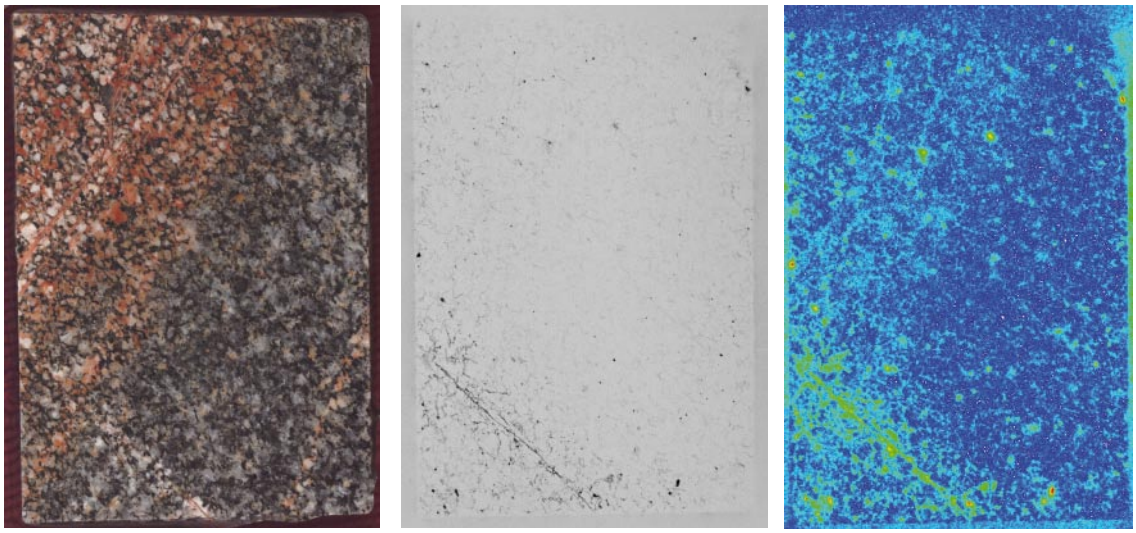

a *b* *c*

Figure 4-31*. a) the analysed rock surface for sample F10B, b) its corresponding film autoradiograph and c) its corresponding digital autoradiograph.*

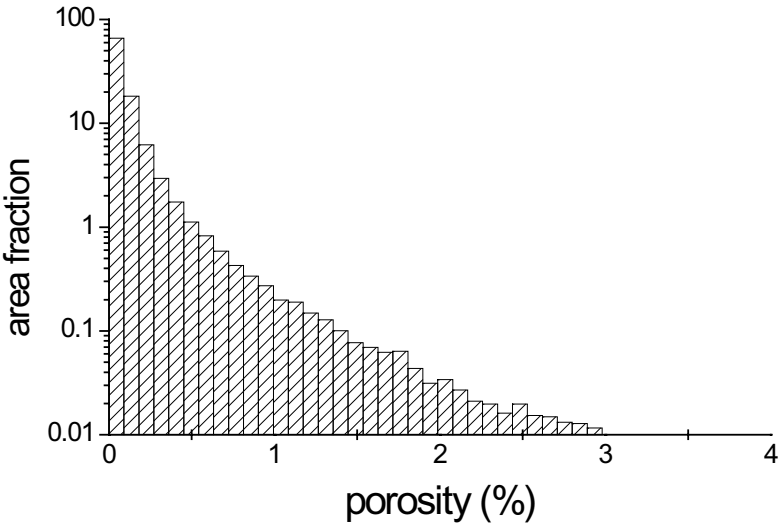

Figure 4-32. *Porosity histogram of sample F10B. A total PMMA porosity of 0.1% was determined.*

4.11 Sample F11 (KFM06B)

The photograph taken of sample F11, before any operation, and the partition diagram are presented in Appendix 11. A photo image of the analysed rock surface after impregnation and sawing is presented below in Figure 4-33a and the corresponding film and digitalauto-radiographs are shown in Figures 4-33b and 4-33c, respectively. The exposure time on the film autoradiograph was 8 days and on the digital autoradiograph 23 hours.

The PMMA porosity for the sample F11 is 10%. The rock sample has been fully impregnated. A few veins consisting of moderately altered mineral grains (maybe some quartz grains) show porosities lower than 2%. The porosity pattern is fairly even; most of the matrix is porous indicating high permeability. The highly altered minerals (maybe chlorites) are most porous in this sample exhibiting porosities of over > 15%. The porosity histogram for the whole sample is shown in Figure 4-34.

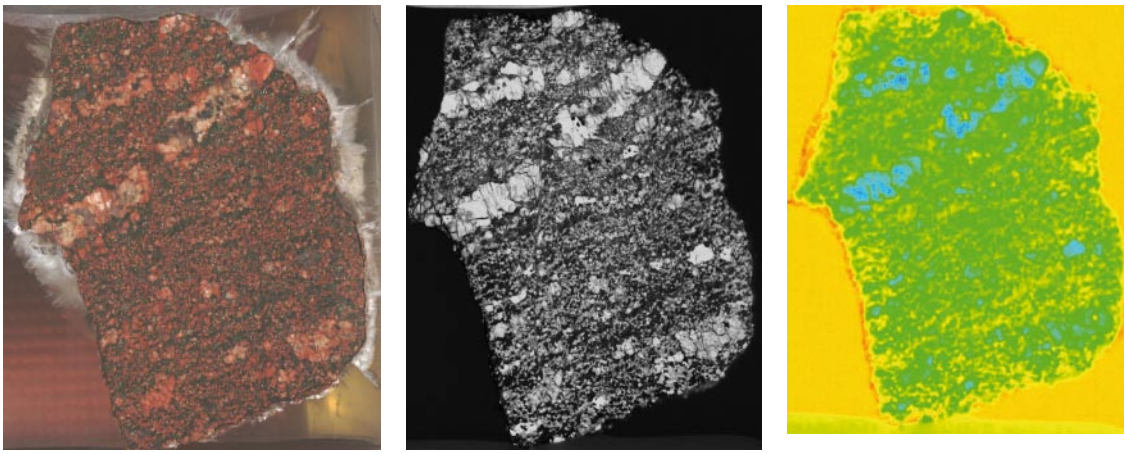

a *b* *c*

Figure 4-33*. a) the analysed rock surface of sample F11, b) its corresponding film autoradiograph and c) its corresponding digital autoradiograph*

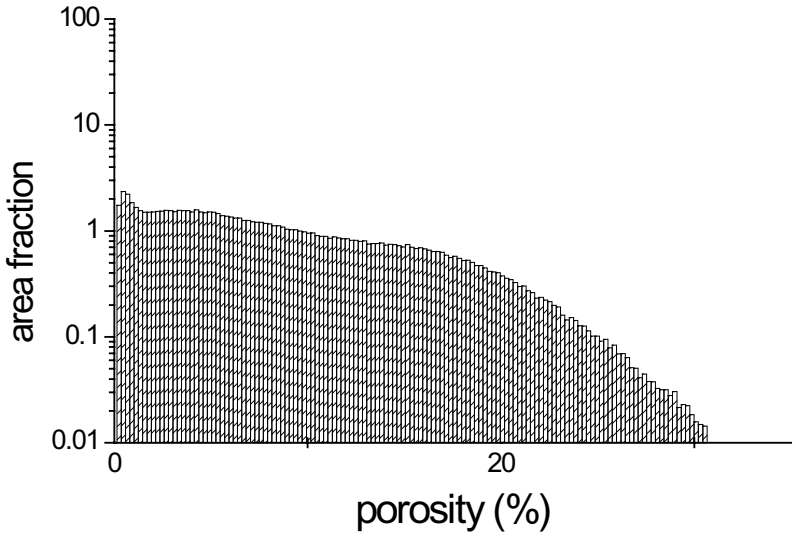

Figure 4-34. *Porosity histogram of sample F11. A total PMMA porosity of 10% was determined.*

4.12 Sample F12 (KFM07A)

The photograph taken of sample F12, before any operation, and the partition diagram are presented in Appendix 12. A photo image of the analysed rock surface after impregnation and sawing is presented below in Figure 4-35a and the corresponding film and digital autoradiographs are shown in Figures 4-35b and 5-35c, respectively. The exposure time on the film autoradiograph was 21 days and on the digital autoradiograph 4 days.

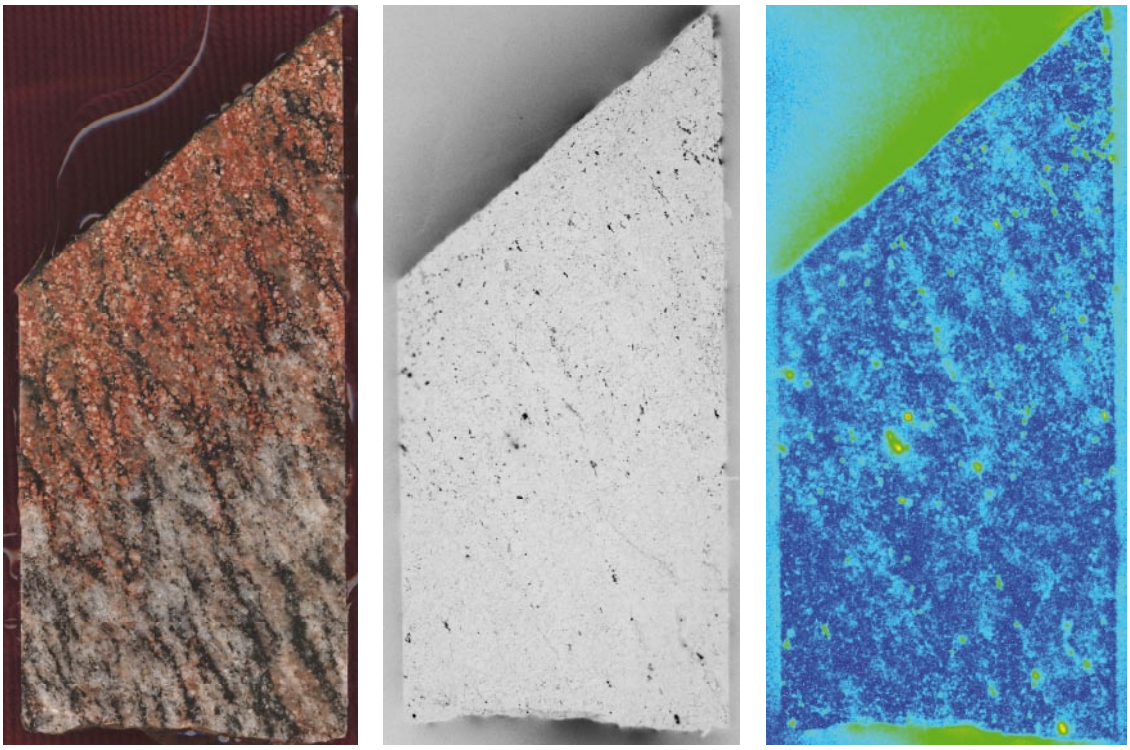

a *b* *c*

Figure 4-35. *a) the analysed rock surface of sample F12, b) its corresponding film autoradiograph and c) its corresponding digital autoradiograph.*

The PMMA porosity result of 0.1% is measured from the upper part of the sample (Figure4-35a, reddish colour in the rock). In this part the rock sample has been fairly well impregnated and shows an even porosity pattern, but not a clear grain boundary porosity. However, the PMMA porosity is very low and matrix is tight, indicating low permeability. The PMMA porosity is less than 0.05% in the lower part of the sample (Figure 4-35a, greyish colour in the rock). Only a few micro fissures are observed. Figure 4-36 shows the porosity histogram for F12 achieved with the PMMA method.

4.13 Sample F13 (KFM07A)

The photograph taken of sample F13, before any operation, and the partition diagram are presented in Appendix 13. A photo image of the analysed rock surface after impregnation and sawing is presented below in Figure 4-37a and the corresponding film and digital autoradiographs are shown in Figures 4-37b and 4-37c, respectively. The exposure time on the film autoradiograph was 25 days and on the digital autoradiograph 4 days.

The PMMA porosity for the F13 sample is 0.2%. Figure 4-38 shows the porosity histogram for F13 achieved with the PMMA method. The rock sample has been fully impregnated; the porosity pattern consists of grain boundary pores as well as intragranular porosity. PMMA rings are found around quartz grains. An even porosity pattern was identified. However, the porosity pattern is found even within this fine grained rock sample. With water gravimetry the porosity for sample F13 was 0.3%. In Figure 4-39 a porosity of over 0.25% is shown in red colour.

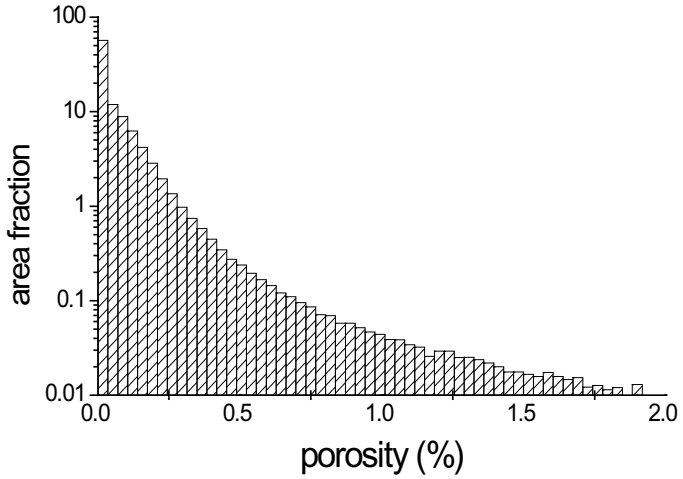

Figure 4-36. *Porosity histogram of sample F12. A total PMMA porosity of 0.1% was determined.*

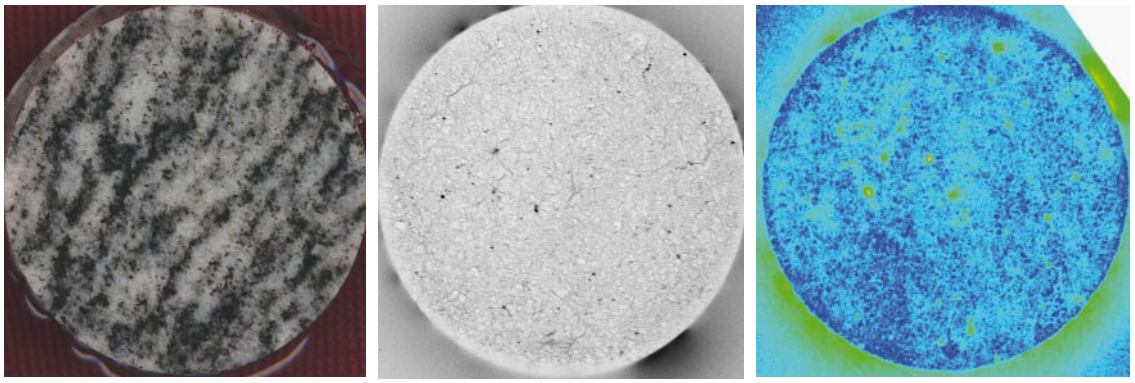

a *b* *c*

Figure 4-37. *a) the analysed rock surface of sample F13, b) its corresponding film autoradiograph and c) its corresponding digital autoradiograph.*

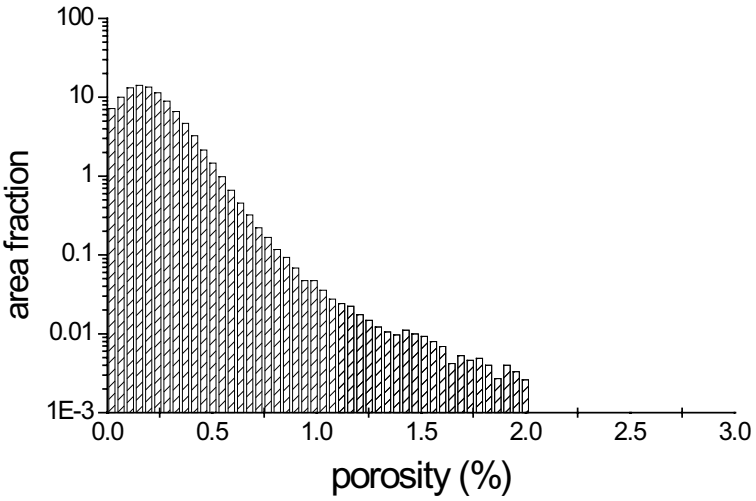

Figure 4-38. *Porosity histogram of sample F13. A total PMMA porosity of 0.2% was determined.*

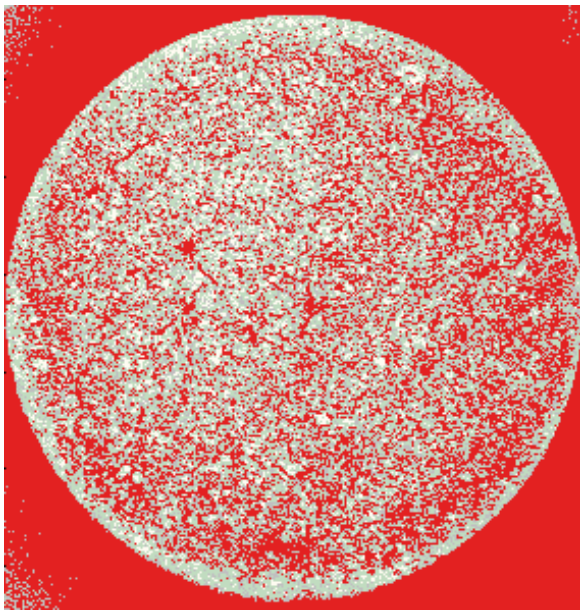

Figure 4-39. *Autoradiograph of sample F13 with a porosity exceeding 0.25% shown in red.*

5 Summary and discussions

Thirteen crystalline rock samples were analysed by the ^{14}C-PMMA method. The method involves impregnation of centimetre-scale rock cores with ^{14}C-labelled methylmethacrylate (^{14}C-MMA) in a vacuum, irradiation polymerisation, sample partitioning, autoradiography, optical densitometry and porosity calculation routines using digital image processing techniques.

The rock types of the samples were granites, granodiorites, tonalities, amphibolites with a variety of their alteration and weathering products. In addition a few samples were taken adjacent to water bearing fracture zones. The PMMA porosities for low porous matrices, i.e. porosities lower than 1%, varied between 0.05% and 0.5% depending on the sample. These samples represent granites, granodiorites and tonalities; fine- to medium-grained unaltered rocks. Sample F10 and F12 contained a fracture zone with an altered wall rock where the PMMA porosity was about 0.1%, indicating very tight and impermeable matrix. The highest porosities were found in samples taken adjacent to the water bearing fractures (F8), altered amphibolite (F4), laumontite sealed breccia (F9) and metamorphic, medium-grained quartz dissoluted granite to granodiorite (F2).

The main focus of the work was to analyze the porosities and visualize the heterogeneous pore structure of crystalline rocks by using ^{14}C-PMMA autoradiographs. The grain boundary porosity was found to dominate in a few samples; F3, F5 and F13. However, in many cases the porosity pattern was not congruent with the mineral texture. The intragranular porosity dominated in samples having high porosities; here 3%–16%. These samples also had very heterogeneous porosity patterns in cm scales. The experiences from this study have shown that the technique can be applied effectively to study the spatial distribution of porosity in low porous media. The porosity profiles adjacent to water bearing fracture zones can also be studied.

As thought in the beginning of the PMMA method development, the MMA molecule is considered to behave in rock as a neutral particle, without strong surface interaction, and it can be roughly compared with water. The presence of residual water and the surface state of the rock pore space are influenced by the pre-treatment (drying and degassing) that the samples undergo before impregnation. Intrusion of MMA, which is a hydrophobic fluid, is hindered if even thin water layers remain absorbed on the rock pore surfaces after drying. The initial expectation was that the above mentioned differences could cause some discrepancy in the porosity values obtained by the PMMA method and water gravimetry. Correlations between water and PMMA porosities are plotted in Figure 4-1. The PMMA porosity values were in most of the cases lower than the porosity values from water gravimetry /5/. Relative to water gravimetry the PMMA method underestimates the porosity values by 10 to–40%.

There are three probable reasons for the lower porosity values measured by the PMMA method. First, the MMA molecule, in contrast to water, may not intrude into the smallest pores of the rock matrix, thus decreasing the porosity values. The finding that the PMMA porosity values are in disagreement with the water porosity values in unaltered rocks, suggests incomplete intrusion of MMA into the narrow pore spaces. Secondly, the sensitivity of the PMMA method is directly dependent on the signal detection: initially the blackening of the autoradiograph, which is dependent on the ^{14}C activity in the rock, and then the image digitising and on the linearity requirement of the digitising equipment. Thus, if the threshold energy for the autoradiography is not exceeded, some concentration of MMA in the rock may go undetected, resulting in the recording of lower porosity values by the PMMA method than by water gravimetry. Thirdly, if the nonlinear region of the calibration curve is used in the PMMA method, the uncertainty for high porosity values increases, lowering the total PMMA porosities.

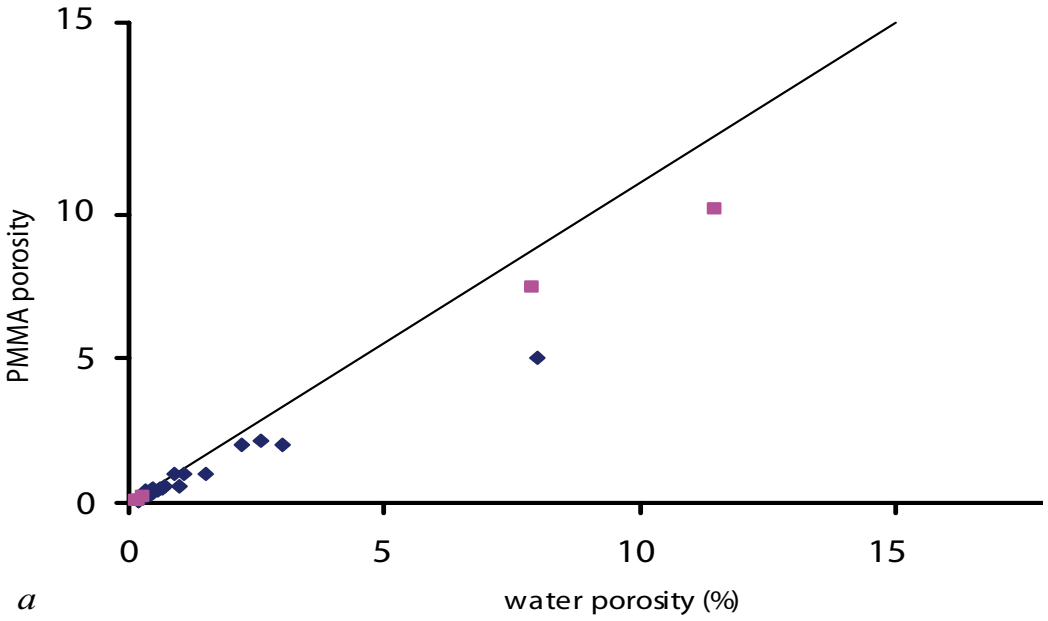

a

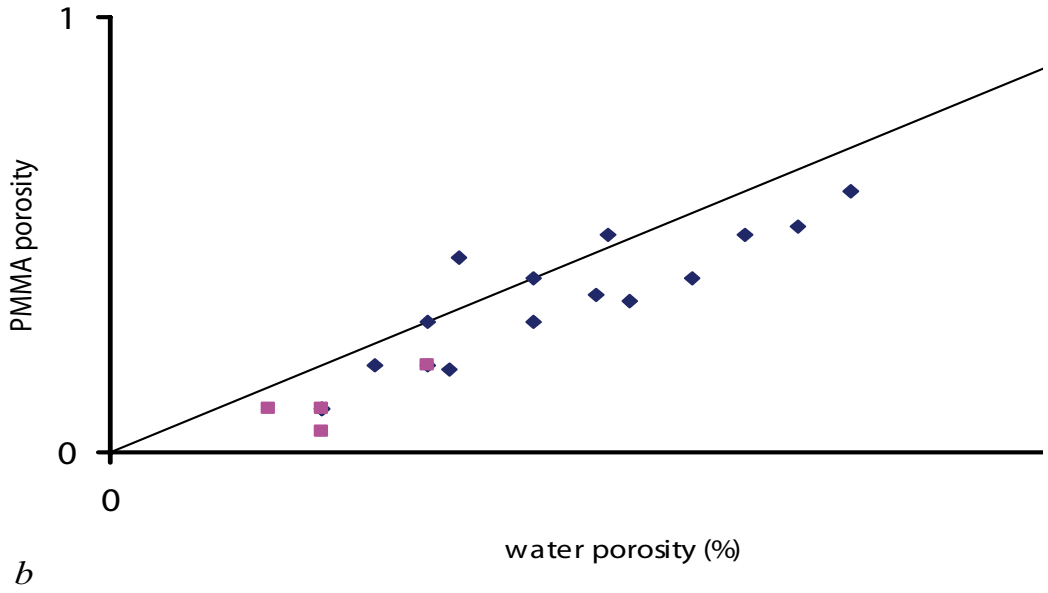

b

Figure 5-1. *Porosity values from water gravimetry compared with PMMA result. a) for rock samples studied previously by Siitari-Kauppi /4/ (blue squares) and in this work (red squares) and b) for the low porosity rocks representing unaltered rocks.*

References

/1/ **Hellmuth K-H, Siitari-Kauppi M, Lindberg A, 1993.** Study of Porosity and Migration Pathways in Crystalline Rock by Impregnation With ^{14}C-Polymethylmethacrylate, Journal of Contaminant Hydrology 13, 403–418

/2/ **Hellmuth K-H, Lukkarinen S, Siitari-Kauppi M, 1994.** Rock Matrix Studies with Carbon-14-Polymethylmethacrylate (PMMA): Method Development and Applications. Isotopenpraxis. Isotopes in Environmental and Health Studies 30, 47–60

/3/ **Hellmuth K-H, Siitari-Kauppi M, Klobes P, Meyer K, Goebbels J, 1999.** Imaging and Aanalyzing Rock Porosity by Autoradiography and Hg-Porosimetry/X-ray Computertomography-Applications, Phys. Chem. Earth (A), Vol. 24, No. 7, 569–573

/4/ **Siitari-Kauppi M, Flitsiyan E S, Klobes P, Meyer K, Hellmuth K-H, 1998.** Progress in Physical Rock Matrix Characterization: Structure of the Pore Space. In: I.G. McKinley, C. McCombie (edits.), Scientific Basis for Nuclear Waste Management XXI, Mat. Res. Soc. Symp. Proc. 506, 671–678

/5/ **Siitari-Kauppi M, 2002.** Development of ^{14}C-Polymethylmethacrylate Method to Characterise Low Porosity Media-Application to Rocks in Geological Barriers of Nuclear Waste Storage. Academic Thesis, UHRAD-17-2002

/6/ **Siitari-Kauppi M, Autio J, 2001.** Study of Rock Damage by Drill and Blast Excavation at the Research Tunnel at Olkiluoto, In Water-Rock Interaction 10, Cidu (ed) Balkema, Lisse, 1387–1390

/7/ **Autio J, Kirkkomäki T, Siitari-Kauppi M, Laajalahti M, Aaltonen T, Maaranen J, 1999.** Use of the ^{14}C-PMMA and He-gas Methods to Characterise Excavation Disturbance in Crystalline Rock, Posiva 99–22 and SKB Report IPR-99–18

/8/ **Daniels F, Alberty R A, 1967.** Physical Chemistry, Third Edition, John Wiley & Sons, Inc. New York, 384 (767)

/9/ **Leonard E C, 1978.** Vinyl and diene monomers, Part 1, A Series of Monographs on the Chemistry, Physics, and Technology of High Polymeric Substances, Vol. XXIV, 157

/10/ **Frieg B, Alexaner W R, Dollinger H, Buhler C, Haag P, Möri A, Ota K, 1998.** In Situ Resin Impregnation or Investigating Radionuclide Retardation in Fractured Repository Host Rocks, Journal of Contaminant Hydrology 35, 115–130

Appendices

Appendix 1 The photo images of sample F1 before any operation and the partition map for PMMA analyses and autoradiography. Shaded surfaces are autoradiographed.

Appendix 2 The photo images of sample F2 before any operation and the partition map for PMMA analyses and autoradiography. Shaded surfaces are autoradiographed.

Appendix 3 The photo images of sample F3 before any operation and the partition map for PMMA analyses and autoradiography. Shaded surfaces are autoradiographed.

Appendix 4 The photo images of sample F4 before any operation and the partition map for PMMA analyses and autoradiography. Shaded surfaces are autoradiographed.

Appendix 5 The photo images of sample F5 before any operation and the partition map for PMMA analyses and autoradiography. Shaded surfaces are autoradiographed.

Appendix 6 The photo images of sample F6 before any operation and the partition map for PMMA analyses and autoradiography. Shaded surfaces are autoradiographed.

Appendix 7 The photo images of sample F7 before any operation and the partition map for PMMA analyses and autoradiography. Shaded surfaces are autoradiographed.

Appendix 8 The photo images of sample F8 before any operation and the partition map for PMMA analyses and autoradiography. Shaded surfaces are autoradiographed.

Appendix 9 The photo images of sample F9 before any operation and the partition map for PMMA analyses and autoradiography. Shaded surfaces are autoradiographed.

Appendix 10 The photo images of sample F10 before any operation and the partition map for PMMA analyses and autoradiography. Shaded surfaces are autoradiographed.

Appendix 11 The photo images of sample F11 before any operation and the partition map for PMMA analyses and autoradiography. Shaded surfaces are autoradiographed.

Appendix 12 The photo images of sample F12 before any operation and the partition map for PMMA analyses and autoradiography. Shaded surfaces are autoradiographed.

Appendix 13 The photo images of sample F13 before any operation and the partition map for PMMA analyses and autoradiography. Shaded surfaces are autoradiographed.

Appendix 14. Presents the initial data given by Geosigma. A short description of sample types and the depths of samples in the borehole are given.

Appendix 15. Lists the experimental procedure for the studied samples.

Appendix 1

Worksheet for sample F1 (KFM01A)

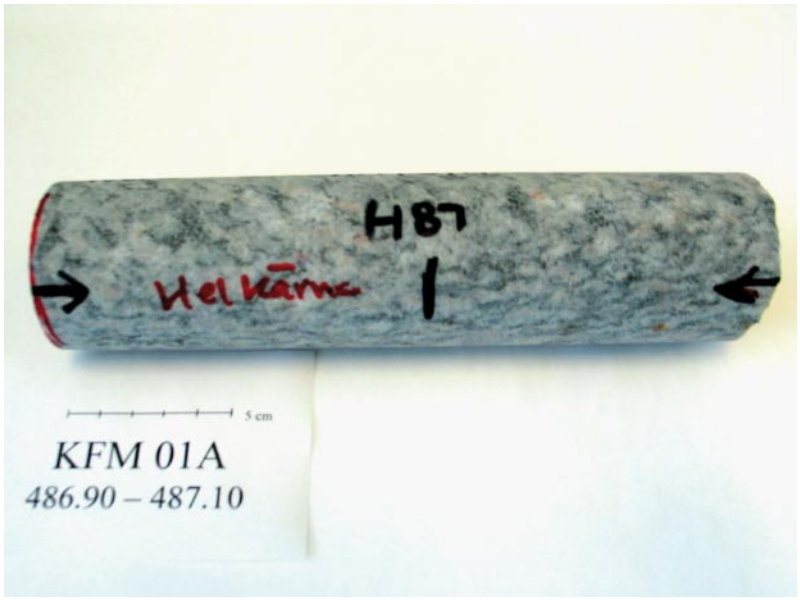

Figure A1-1. *The whole sample before analysis.*

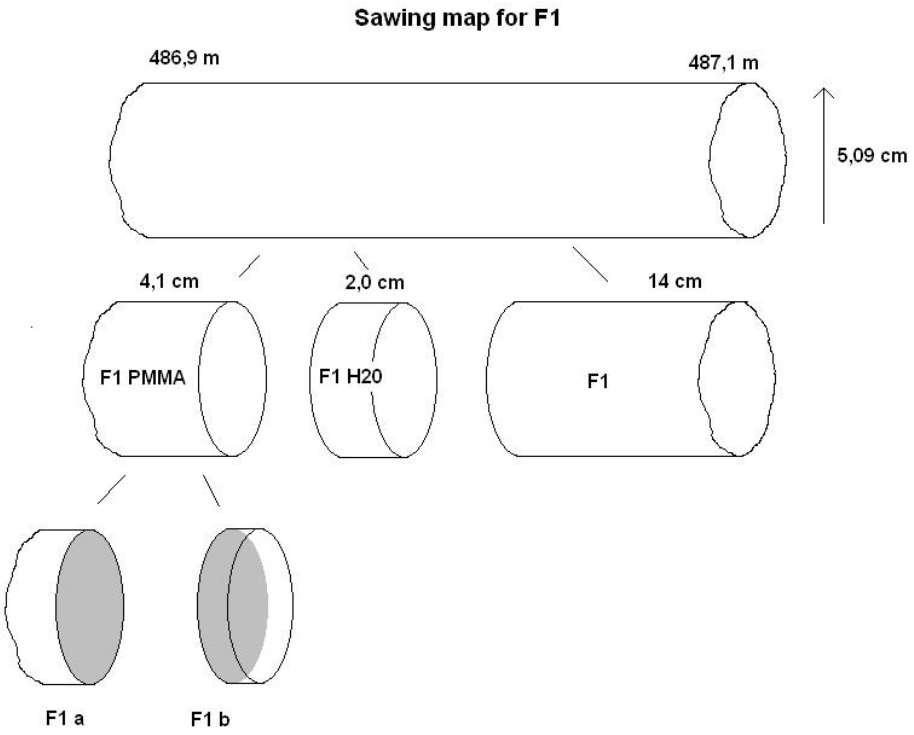

Figure A1-2. *Partition diagram for sample F1.*

Appendix 2

Worksheet for sample F2 (KFM02A)

Figure A2-1. *The whole sample before analysis.*

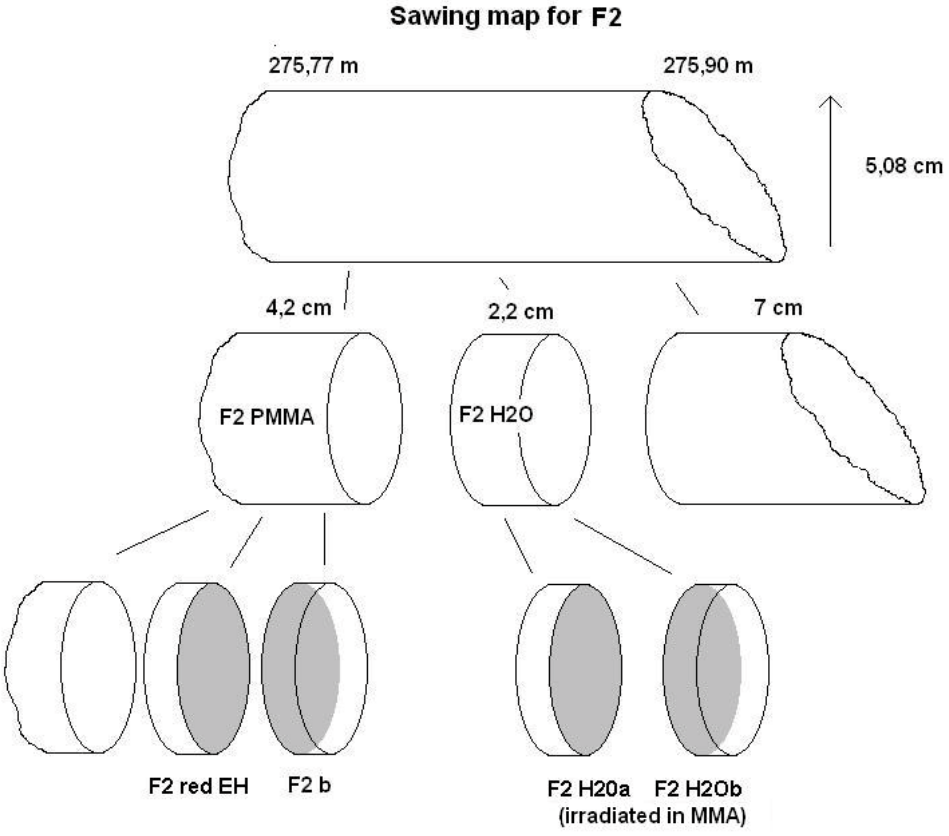

Figure A2-2. *Partition diagram for sample F2.*

Appendix 3

Worksheet for sample F3 (KFM02A)

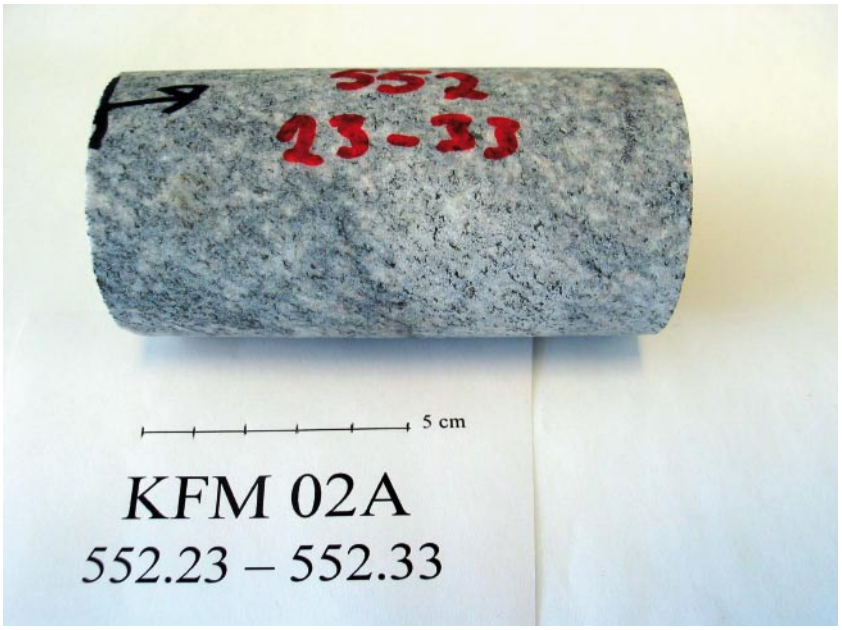

Figure A3-1. *The whole sample before analysis.*

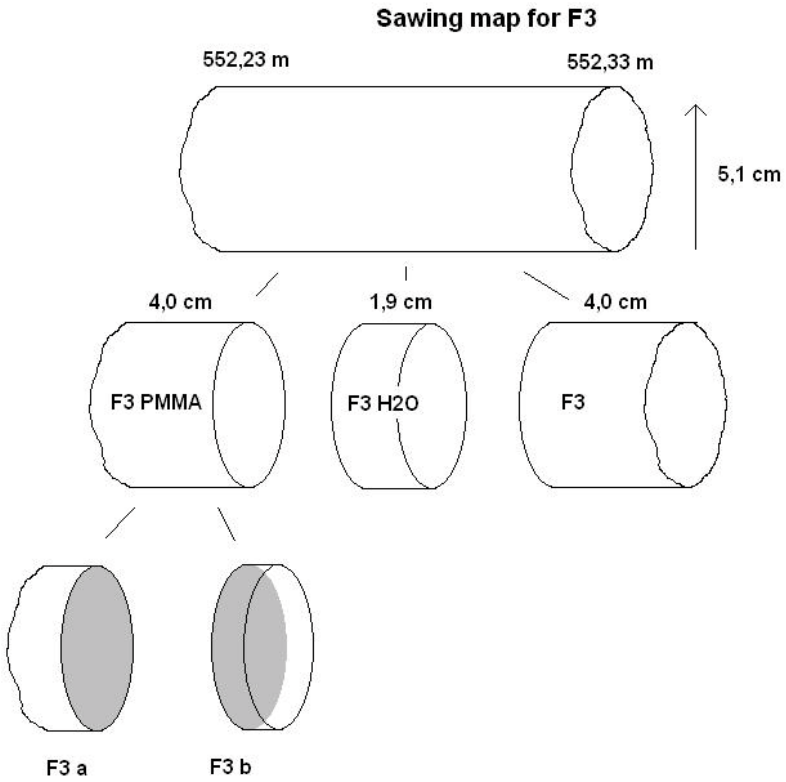

Figure A3-2. *Partition diagram for sample F3.*

Appendix 4

Worksheet for sample F4 (KFM04A)

Figure A4-1. *The whole sample before analysis.*

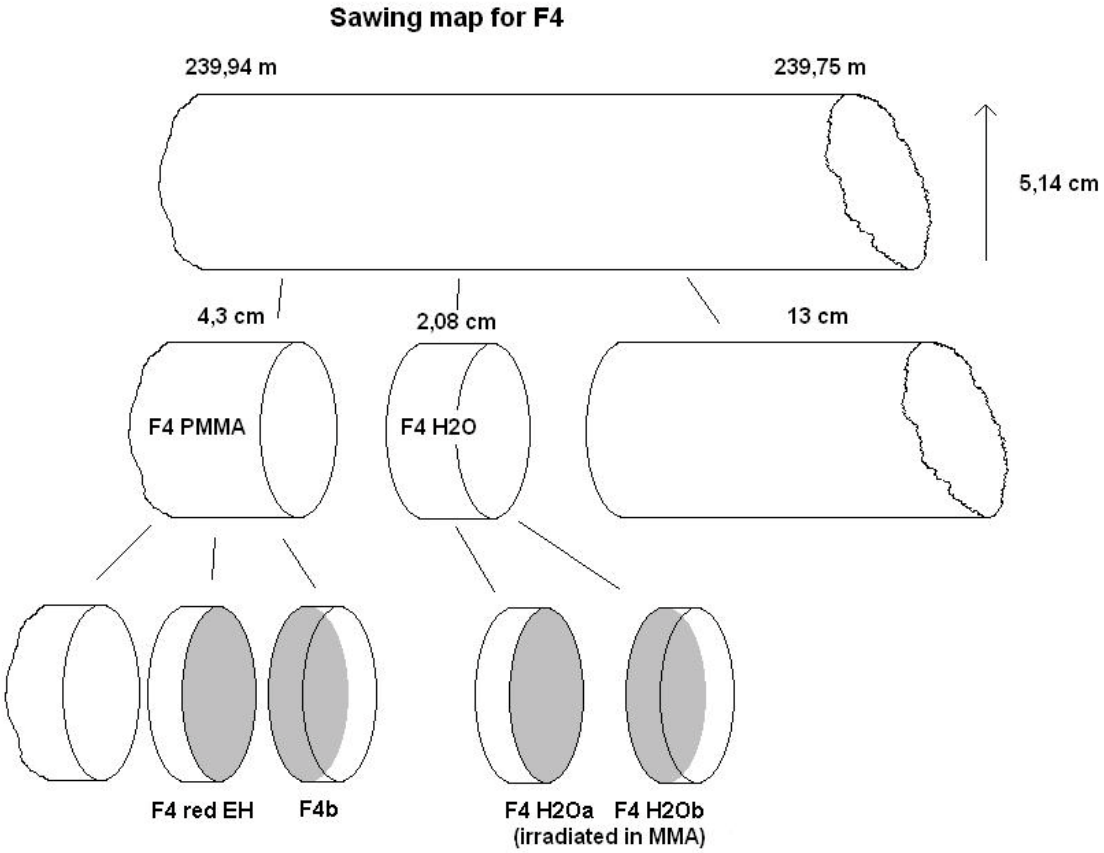

Figure A4-2. *Partition diagram for sample F4.*

Appendix 5

Worksheet for sample F5 (KFM05A)

Figure A5-1. *The whole sample before analysis.*

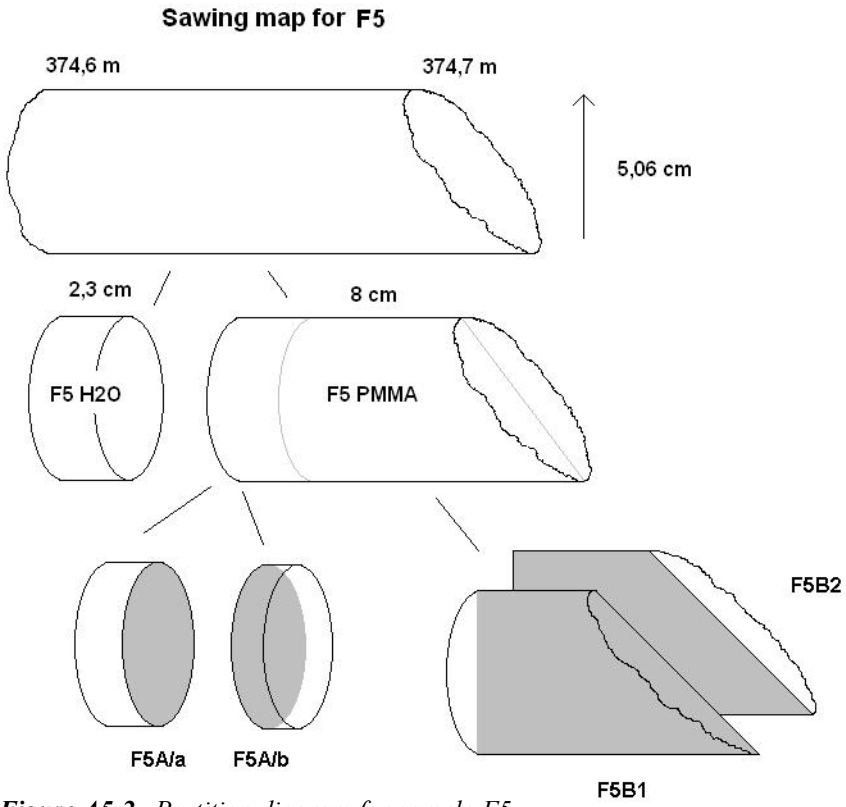

Figure A5-2. *Partition diagram for sample F5.*

Appendix 6

Worksheet for sample F6 (KFM03A)

Figure A6-1. *The whole sample before analysis.*

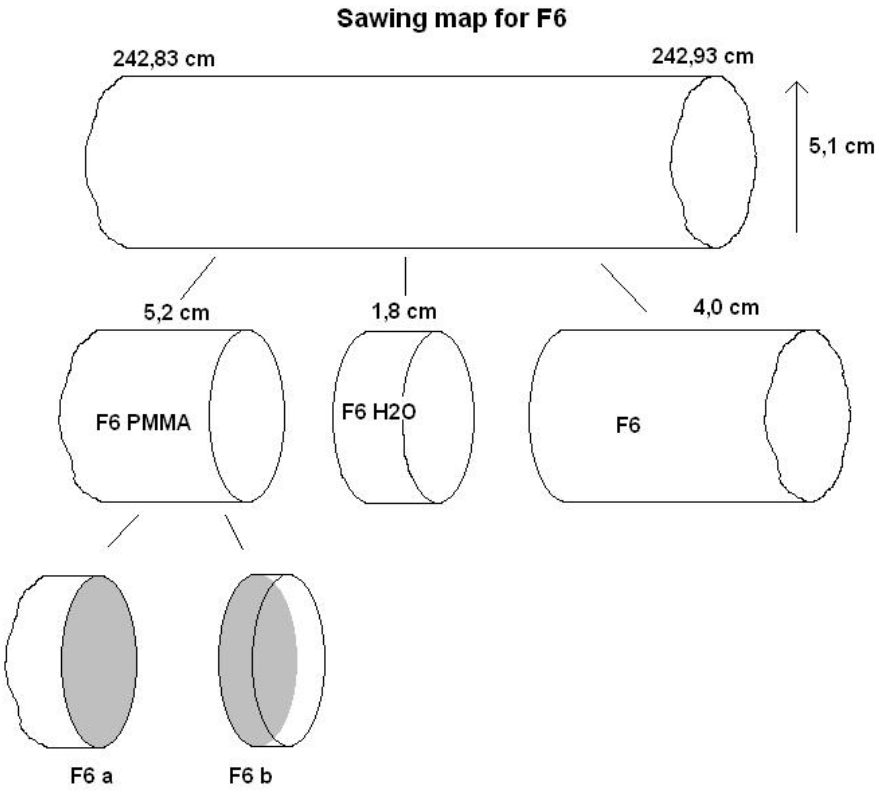

Figure A6-2. *Partition diagram for sample F6.*

Appendix 7

Worksheet for sample F7 (KFM04A)

Figure A7-1. *The whole sample before analysis.*

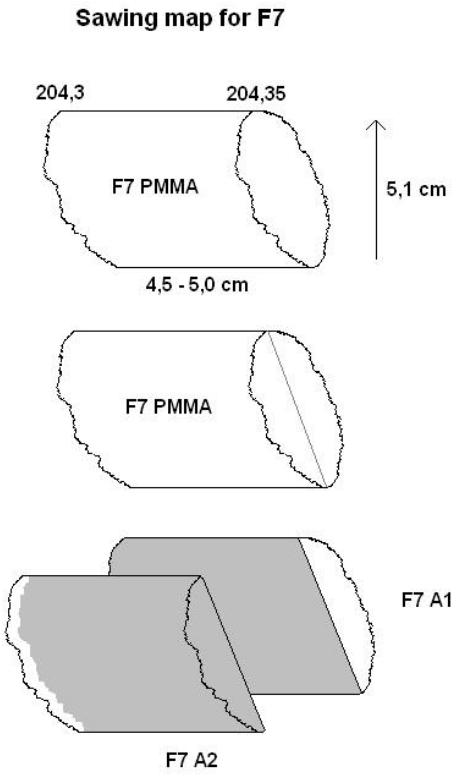

Figure A7-2. *Partition diagram for sample F7.*

Appendix 8

Worksheet for sample F8 (KFM04A)

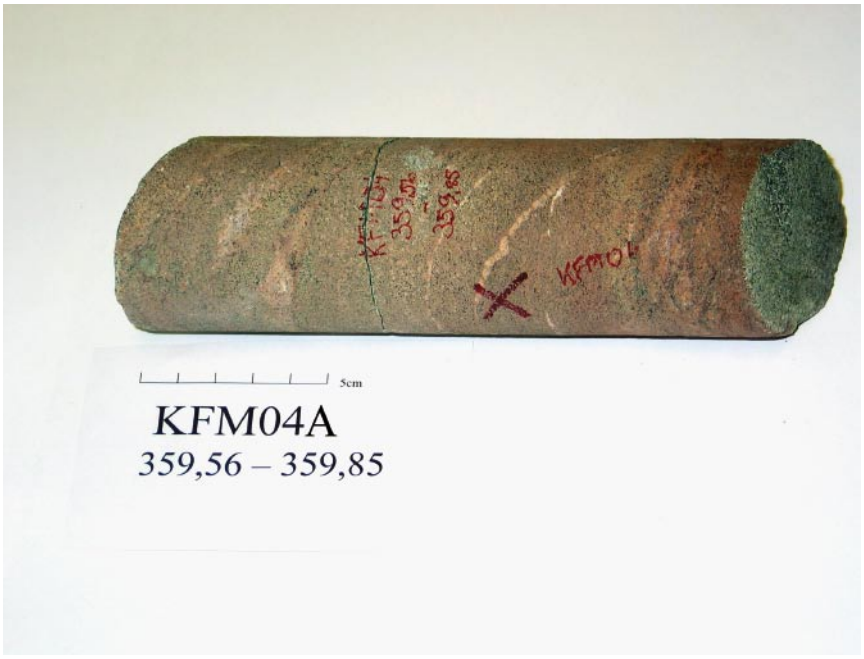

Figure A8-1. *The whole sample before analysis.*

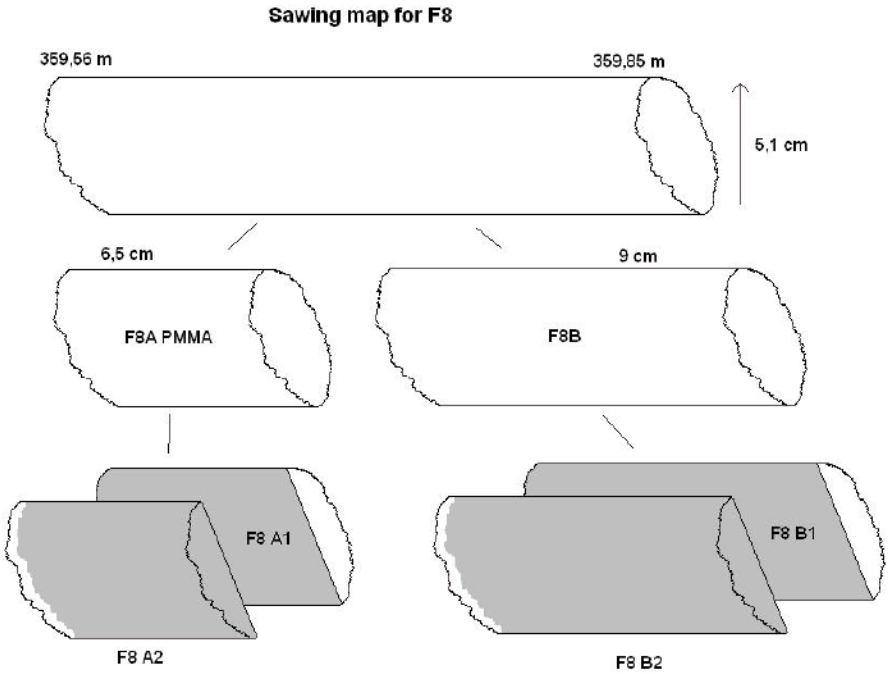

Figure A8-2. *Partition diagram for sample F8.*

Appendix 9

Worksheet for sample F9 (KFM05A)

Figure A9-1. *The whole sample before analysis.*

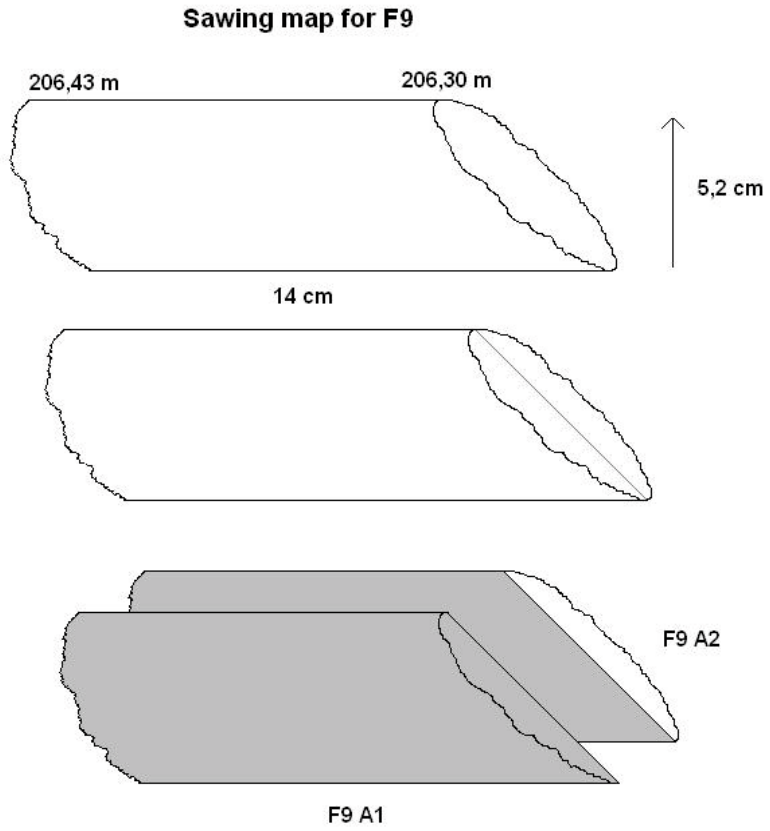

Figure A9-2. *Partition diagram for sample F9.*

Appendix 10

Worksheet for sample F10 (KFM05A)

Figure A10-1. *The whole sample before analysis.*

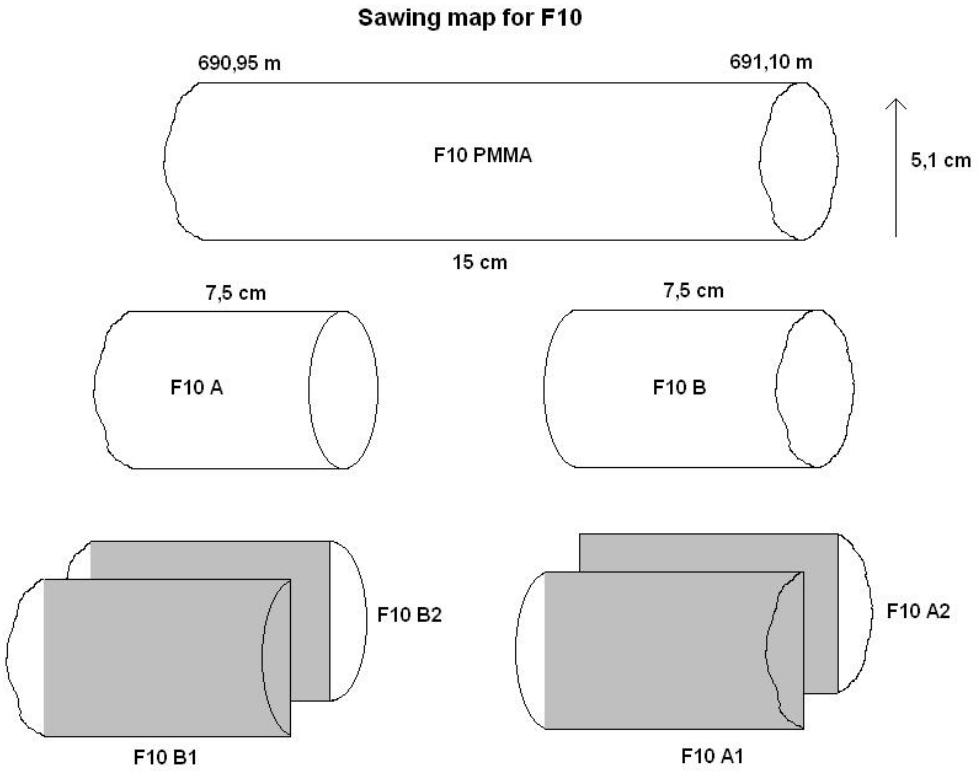

Figure A10-2. *Partition diagram for sample F10.*

Appendix 11

Worksheet for sample F11 (KFM06B)

Figure A11-1. *The whole sample before analysis.*

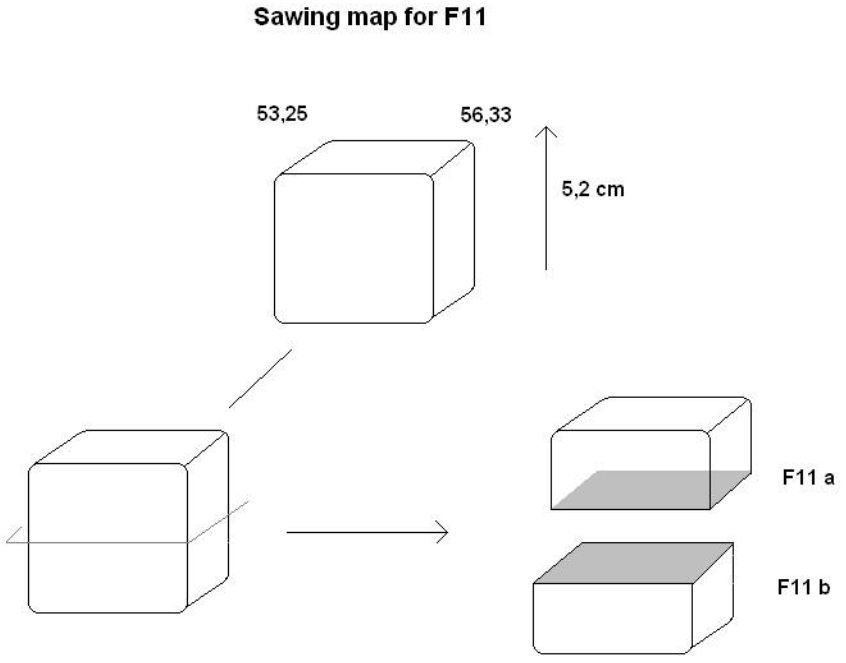

Figure A11-2. *Partition diagram for sample F11.*

Appendix 12

Worksheet for sample F12 (KFM07A)

Figure A12-1. *The whole sample before analysis.*

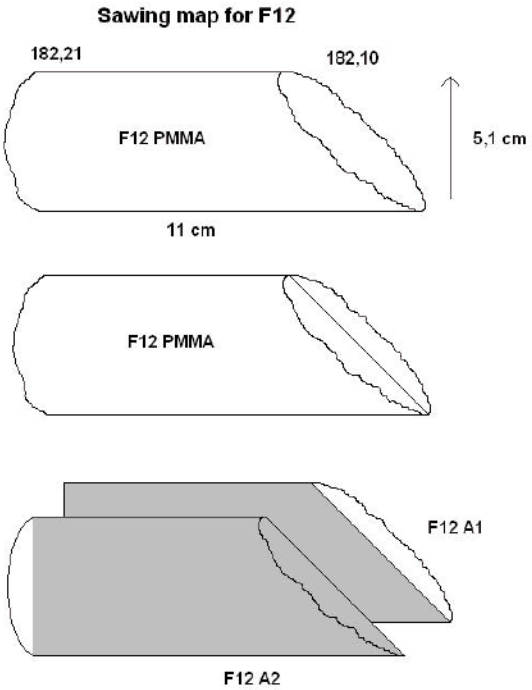

Figure A12-2. *Partition diagram for sample F12.*

Appendix 13

Worksheet for sample F13 (KFM07A)

Figure A13-1. *The whole sample before analysis.*

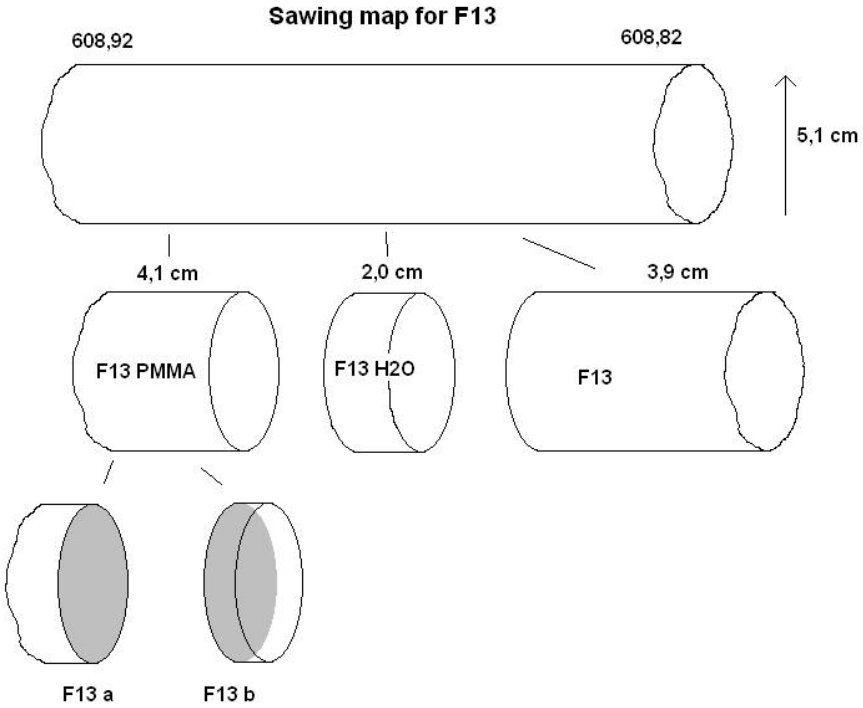

Figure A13-2. *Partition diagram for sample F13.*

Appendix 14

The initial data given by SKB

A short description of sample types and the depths of samples in the borehole are given.

HYRL code	Borehole	Secup	Seclow	Rock type	Comments
F1	KFM01A	486.90	487.10	Granite to granodiorite, metamorphic, medium-grained	
F2	KFM02A	275.77	275.9	Granite to granodiorite, metamorphic, medium-grained,	Quartz dissoluted (“episyenite”)
F3	KFM02A	552.23	552.33	Granite, granodiorite and tonalite, metamorphic, fine- to medium-grained	
F4	KFM04A	239.75	239.94	Amphibolite	Strong alteration
F5	KFM03A	374.6	374.70	Pegmatite, pegmatitic granite	
F6	KFM03A	242.83	242.93	Tonalite to granodiorite, metamorphic	
F7	KFM04A	204.30	204.35	Granite to granodiorite, metamorphic, medium-grained	Wall rock alteration
F8	KFM04A	359.56	359.85	Granite, granodiorite and tonalite, metamorphic, fine- to medium-grained	Sample from water conducting zone
F9	KFM05A	206.3	206.43	Granite to granodiorite, metamorphic, medium-grained	Brecciated bed-rock, sealed with laumontite
F10	KFM05A	690.95	691.10	Granite, granodiorite and tonalite, metamorphic, fine- to medium-grained	Sealed fractures with bedrock alteration
F11	KFM06B	56.25	56.33	Granite to granodiorite, metamorphic, medium-grained	Altered bedrock
F12	KFM07A	182.10	182.21	Granite to granodiorite, metamorphic, medium-grained	Open fracture with altered wall rock
F13	KFM07A	608.82	608.92	Granite to granodiorite, metamorphic, medium-grained	

Appendix 15

The experimental procedure for the studied Forsmark samples

HYRL code	SKB code	Length (mm)	Diameter (mm)	Drying time (d)	Drying temp (ºC)	Tracer activity (kBq/ml)	Impregna-tion (d)	Radiation dose (kGy)	Exposure time (d)
F1	KFM 01A	41	51	9	95 ± 5	~ 520	25	75	21d
F2	KFM 02A	42	51	4	40 ± 5	~ 40	22	77	7d
		22		3	85 ± 5	~ 40	13	68	7d
F3	KFM 02A	40	51	26	95 ± 5	~ 520	30	69	21d
F4	KFM 04A	43	51	4	40 ± 5	~ 40	22	77	7d
		21		3	85 ± 5	~ 40	13	68	7d
F5	KFM 05A	80	51	26	95 ± 5	~ 520	30	69	21d
F6	KFM 03A	40	51	19	98 ± 5	~ 260	30	81	25d
F7	KFM 04A	50	51	17	74 ± 5	~ 190	29	95	14d
F8A	KFM 04A	45	51	7	88 ± 5	~ 560	40	88	4d
F8B		110		7	93 ± 5	~ 930	16	73	4d
F9	KFM 05A	120	52	7	91± 5	~ 40	21	95	7d
F10	KFM 05A	150	51	11	92 ± 5	~ 190	19	81	20d
F11	KFM 06B	50	52	17	74 ± 5	~ 190	29	79	8d
F12	KFM 07A	88	51	11	88 ± 5	~ 190	19	81	21d
F13	KFM 07A	41	51	19	98 ± 5	~ 260	30	81	25d